applied sciences

MDPI

Article

Maleic Anhydride-Derived Copolymers Conjugated with Beta-Lactam Antibiotics: Synthesis, Characterization, In Vitro Activity/Stability Tests with Antibacterial Studies

Aysegul Kahraman, Dolunay Sakar * and Melda Altikatoglu Yapaoz

Chemistry Department, Art and Science Faculty, Yildiz Technical University, 34220 Istanbul, Türkiye; f7217001@std.yildiz.edu.tr (A.K.); malti@yildiz.edu.tr (M.A.Y.)
* Correspondence: dsakar@yildiz.edu.tr

Abstract: The synthesis and characterization of biocompatible three different maleic anhydride copolymer conjugated with two different beta-lactam antibiotics at in vitro conditions were conducted. The polymer–drug conjugates were synthesized by coupling β-lactam antibiotics via amide bonds to the copolymer. In this work, six different drug-functionalized maleic anhydride copolymers (DFMACs) were synthesized by the chemical conjugation method. This method is based on the ring-opening reaction of the anhydride ring of the copolymer to form an amide bond linking the drug. The synthesized DFMACs were characterized by ^{1}H NMR and FTIR/ATR spectroscopies and analyses were carried out by UV/VIS spectroscopy and Zeta-sizer instrument in detail with consecutive antibacterial tests. The existence of a newly formed amide covalent bond between the drug and the copolymer chains was confirmed by ^{1}H NMR and FTIR/ATR studies. This is the first report on the application of the selected branched biodegradable polymeric matrices for the covalent conjugation of ampicillin and cefalexin. Optimum stability and activity conditions for the synthesized DFMACs were determined. Analyses were conducted under in vitro conditions including varying pH values and simulated body fluids as a function of time to obtain new drug delivery system candidates for the two different antibiotics.

Keywords: maleic anhydride-derived copolymers; beta-lactam antibiotics; drug-functionalized maleic anhydride copolymers (DFMACs)

check for updates

Citation: Kahraman, A.; Sakar, D.; Altikatoglu Yapaoz, M. Maleic Anhydride-Derived Copolymers Conjugated with Beta-Lactam Antibiotics: Synthesis, Characterization, In Vitro Activity/Stability Tests with Antibacterial Studies. *Appl. Sci.* **2024**, *14*, 6112. https://doi.org/10.3390/app14146112

Academic Editor: Jinchul Kim

Received: 18 May 2024
Revised: 4 July 2024
Accepted: 9 July 2024
Published: 13 July 2024

Copyright: © 2024 by the authors. Licensee MDPI, Basel, Switzerland. This article is an open access article distributed under the terms and conditions of the Creative Commons Attribution (CC BY) license (https://creativecommons.org/licenses/by/4.0/).

1. Introduction

Beta-lactam antibiotics have been the most prominent defense worldwide [1] and have been chosen as one of the essential medicines by the World Health Organization (WHO) [2] for the treatment of bacterial infections. Beta-lactam antibiotics inhibit bacterial cell membrane synthesis showing an antibacterial effect [3]. In this research, ampicillin trihydrate and cefalexin monohydrate were selected for the synthesis of drug-functionalized maleic anhydride copolymers (DFMACs). Those antibiotics were chosen from two subgroups: penicillins (ampicillin) and cephalosporins (cefalexin) to understand the behavior of β-lactam antibiotics in general.

Although cefalexin (CEF) [4] and ampicillin (AMP) are widely used, broad-spectrum antibiotics, they have poor pharmacokinetics. In the treatment of chronic infections, high dosages of antibiotics can cause cumulative toxicity and a burden on the kidneys [4]. Additionally, antibiotic resistance can develop due to the poor pharmacological properties of drugs [5]. Therefore, it is crucial that the pharmacological properties of these antibiotics, such as stability, activity and polydispersity, should be improved while maintaining antibacterial effect. Bioactive polymeric materials are suitable candidates for enhancing the physical and pharmacological properties of drugs [6] due to their desirable properties such as lower dosages and better stability [7]. Although there have been several methods to prepare bioactive polymeric materials, the chemical conjugation method steps forth with

an increased drug loading capacity [8]. The pharmacokinetics of the polymer–drug conjugation often mirror the pharmacokinetics of the polymer itself [9]. Therefore, candidate polymers as drug conjugates should meet certain criteria such as biocompatibility, possessing suitable functional groups like -COOH, -NH_2, -OH, etc., for covalent conjugation with drugs, water solubility, a low PDI value and be readily available [10]. Maleic anhydride-derived polymers meet these criteria for improving the pharmacological properties of drugs due to their special properties [11].

Maleic anhydride copolymers are notable for their unique properties such as biocompatibility, low toxicity [12,13], easy availability, ability to vary hydrophilicity and hydrophobicity depending on comonomer choice and water solubility in pharmaceutical and medical applications [14,15]. Thus, it is possible to modify and enhance properties and usage areas of this class of polymers [11]. Additionally, the chemical structure allows mild reactions with drugs avoiding contamination with impurities [15]. Reactivity of the anhydride group with nucleophilic agents (OH, NH) and reproducible structures [16] make the maleic anhydride copolymers a suitable candidate. The drugs can be attached to maleic anhydride copolymers with ease, either through the anhydride cycle or through the comonomer reactive groups [14,15]. There are many examples of maleic anhydride-based materials used as adhesives, biomedical devices and drug delivery systems in the literature [17–19]. Maleic anhydride copolymers can be used as drugs, as a support to bioactive molecules or as conjugates in drug-controlled release systems [15]. The covalent binding of drugs to macromolecular structures such as polymers forms polymer–drug conjugates. One of the main aims of the usage of polymer–drug conjugates is to enhance the properties of the selected drug in terms of stability, activity, bioavailability, etc. [20]. One of the maleic anhydride-derived copolymers (poly(styrene-alt-maleic anhydride) was covalently conjugated with acetaminophen drug to improve the pharmacological properties [21]. Therefore, in this study, three different maleic anhydride copolymers were chosen for their varying degrees of hydrophilicity: poly(methyl vinyl alt-maleic anhydride) (PMVEMA), poly(ethylene alt-maleic anhydride) (PEMA) and poly(isobutylene alt-maleic anhydride) (PIBMA).

As Smith and co-workers highlighted the need to improve the pharmacological properties of antibiotics [22], we have functionalized three different maleic anhydride copolymers with AMP and CEF from different β-lactam sub-groups, via chemical conjugation. The pharmacological properties of DFMACs such as stability, particle size, PDI and activity were determined under in vitro conditions. Analyses at different pH values and in simulated body fluids over time via Zeta-sizer and UV/VIS measurements were conducted, in addition to the antibacterial tests. The obtained novel DFMACs were evaluated and compared in detail.

2. Materials and Methods

2.1. Chemicals

Poly(methyl vinyl ether-alt-maleic anhydride) (PMVEMA) (Mw ≃ 210,000 g/mol, Mn = 80,000 g/mol, Sigma-Aldrich, St. Louis, MO, USA), poly(isobutylene-alt-maleic anhydride) (PIBMA) (average Mw ~6000, 12–200 mesh, Sigma-Aldrich, St. Louis, MO, USA), poly(ethylene-alt-maleic anhydride) (PEMA) (average Mw 100,000–500,000, Sigma-Aldrich, St. Louis, MO, USA), ampicillin trihydrate (AMP) (BILIM Pharmaceuticals, Istanbul, Turkiye) (99.5% purity), cefalexin monohydrate (CEF) (BILIM Pharmaceuticals, Istanbul, Turkiye) (99.6% purity), N, N-Dimethylformamide (DMF) (≥99.8%, Merck, New York, NY, USA), toluene (Merck, New York, NY, USA) and dimethyl sulfoxide (DMSO) (≥99.9%, Merck, New York, NY, USA) were used in the chemical reactions.

2.2. Synthesis of DFMACs

The anhydride ring of maleic anhydride is prone to nucleophilic attacks by amino or hydroxyl groups [23]. Theoretically, it is expected that the amino groups of ampicillin

trihydrate and cefalexin monohydrate attack the anhydride ring and as a result a ring-opening reaction occurs.

As a reaction procedure for PMVEMA-AMP (Figure 1a), a ring-opening reaction took place by dissolving the PMVEMA copolymer and AMP drug in dimethyl formamide (DMF) at a 1:1 molar ratio and mixing them under inert conditions for 7 days at 70 °C degrees. After the reaction, toluene was added and the mixture was rota-evaporated at 110 °C under vacuum and a drug-functionalized maleic anhydride copolymer was obtained. As a reaction procedure for PIBMA-AMP (Figure 1b), PIBMA and AMP were dissolved in DMF at a 1:1 molar ratio and mixed under inert conditions for 7 days at 70 °C. After the completion of the reaction, toluene was added and the mixture was then rota-evaporated at 110 °C under vacuum. As a reaction procedure for PEMA-AMP (Figure 1c), PEMA and AMP were dissolved in DMF at a 1:1 molar ratio and mixed for 7 days at 70 °C under inert atmosphere. After the completion of the reaction, toluene was added and the mixture was then rota-evaporated at 110 °C under vacuum.

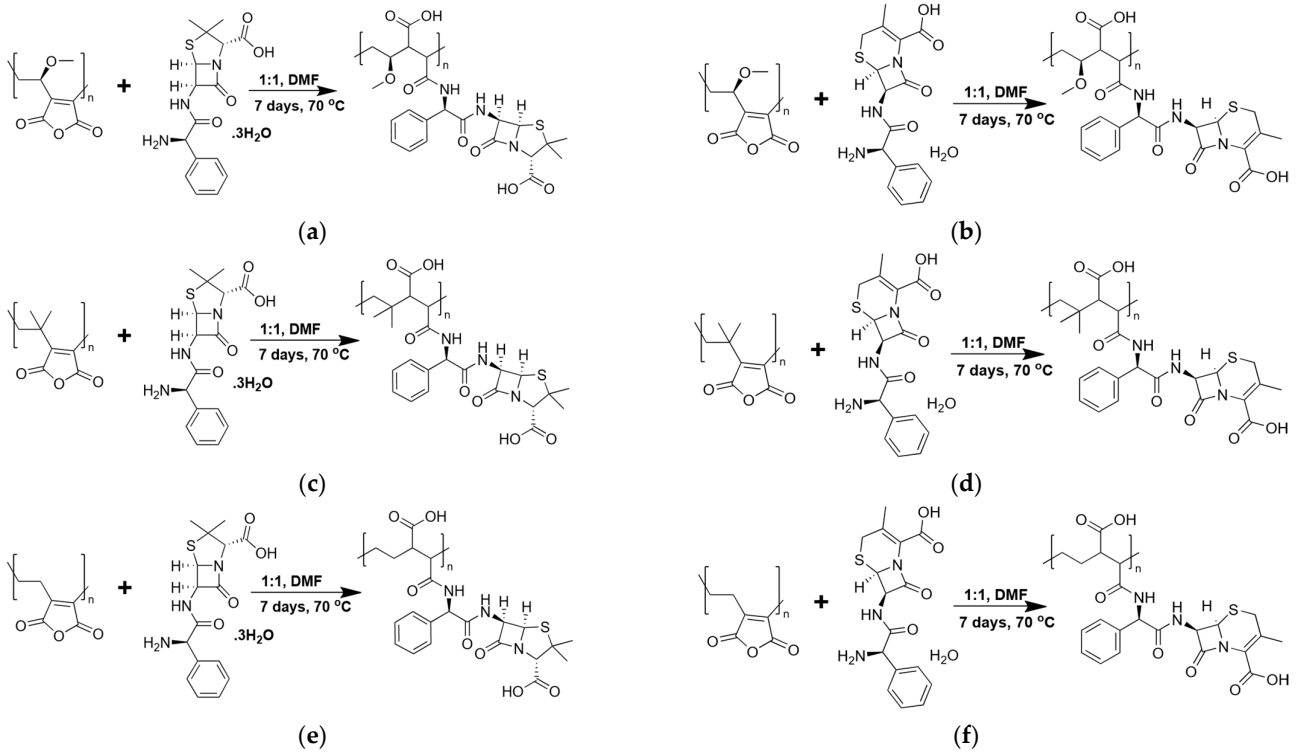


Figure 1. Synthesis routes of PMVEMA-AMP (**a**), PIBMA-AMP (**b**), PEMA-AMP (**c**), PMVEMA-CEF (**d**), PIBMA-CEF (**e**), PEMA-CEF (**f**).

As a reaction procedure for PMVEMA-CEF (Figure 1d), PMVEMA and CEF were dissolved in DMF at a 1:1 molar ratio and mixed for 7 days at 70 °C under inert atmosphere. After the completion of the reaction, toluene was added and the mixture was then rota-evaporated at 110 °C under vacuum. As a reaction procedure for PIBMA-CEF (Figure 1e), PIBMA and CEF were dissolved in DMF at a 1:1 molar ratio and mixed for 7 days at 70 °C under inert atmosphere After the completion of the reaction, toluene was added and the mixture was then rota-evaporated at 110 °C under vacuum. As a reaction procedure for PEMA-CEF (Figure 1f), PEMA and CEF were dissolved in DMF at a 1:1 molar ratio and mixed for 7 days at 70 °C under inert atmosphere. After the completion of the reaction, toluene was added and the mixture was then rota-evaporated at 110 °C under vacuum. These synthesis routes for each of the DFMACs are shown in Figure 1.

Amino groups of AMP and CEF were reacted with the anhydride group of the polymers in Figure 1 and six different drug-functionalized maleic anhydride copolymers were obtained under pre-determined reaction conditions. The yields of DFMACs were calculated

as 74% of PMVEMA-AMP, 65% of PIBMA-AMP, 68% of PEMA-AMP, 70% of PMVEMA-CEF, 63% of PIBMA-CEF and 75% of PEMA-CEF.

2.3. Structural Characterization

Infrared (IR) analyses were performed with a Thermo Fisher Scientific Nicolet iS10 model Fourier transform infrared (FTIR) spectrometer (Waltham, MA, USA) equipped with a Smart iTR model ATR (attenuated total reflectance) apparatus (FTIR/ATR) and DTGS KBr detector. Analyses were conducted between 4000 cm^{-1} and 600 cm^{-1} wave numbers with 32 scans. Air baseline correction was carried out. Results were saved as %Transmittance-Wavenumber (cm^{-1}). All analyses were conducted at 20 °C.

An Agilent 400 MHz Varian VNMRS instrument was used for proton NMR (^{1}H NMR) characterization. Samples were prepared by dissolving compounds in DMSO-d6 as the solvent. All analyses were conducted at 20 °C.

2.4. Stability and Activity Measurements

To measure the polydispersity index, particle size and zeta potential values, a Zeta-sizer (Brookhaven Instruments 90 Plus Particle Size Analyzer, Holtsville, NY, USA) was used. The Smoluchowski model was selected for zeta potential measurements using an SR-542 probe (Brookhaven Instruments 90 Plus Particle Size Analyzer, Holtsville, NY, USA). The Zeta-sizer device automatically provided the particle size, polydispersity, mobility and zeta potential values for the samples. The particle size, zeta potential, and mobility data shown in the table represent averages obtained from 10 measurements, all generated automatically by the device. To evaluate the significance of pH changes and time changes in simulated body fluids at the Zeta-sizer measurements of the samples, the standard deviation and uncertainty values based on Zeta-sizer measurements of the samples were calculated.

Estimated standard uncertainty (U) was calculated by the ratio of estimated standard deviation (SD) to the square root of number of measurements (n) [24], as shown in Equation (1).

$$U = \frac{SD}{\sqrt{n}} \quad (1)$$

In this research, the (n) value represented the number of pH values and time points, which is equal to 12. Standard deviation values and estimated standard uncertainty values of samples were calculated and appended to the last rows of tables in the Zeta-sizer analysis part.

A Sentek P14/BNC electrode (Sentek, Braintree, UK) was utilized for pH measurements. All analyses were conducted at 37 °C degrees to mimic body temperature.

The activity of samples was determined by using a Shimadzu UVmini-1240 model UV/VIS spectrophotometer instrument (Kyoto City, Japan) with Hellma 100-QS quartz cuvette (Müllheim im Markgräflerland, Germany). Analyses were conducted in a wavelength range between 600 nm and 190 nm with 0.5 nm increments between each scan. The baseline correction was conducted against ultra-pure water, PBS (phosphate buffer saline) solution, 0.9% isotonic sodium chloride solution or 5% dextrose solution depending on the type of sample. Samples were prepared as homogenous, liquid solutions. Results were saved in the form of absorbance–wavelength (nm). All samples were analyzed at 37 °C to mimic the body temperature.

2.5. Sample Preparation for Zeta-Sizer and UV/VIS Measurements

Standard sample solutions of PMVEMA (I), PIBMA (II), PEMA (III), AMP (A), CEF (C), PMVEMA-AMP (I-A), PMVEMA-CEF (I-C), PIBMA-AMP (II-A), PIBMA-CEF (II-C), PEMA-AMP (III-A) and PEMA-CEF (III-C) were prepared by dissolving the samples in 5% (v/v) DMSO and mixing them with distilled water for pH measurements. The pH values were adjusted by the addition of various concentrations of NaOH and HCl solutions.

In order to mimic body fluids, these samples were dissolved in 5% (v/v) DMSO, were transferred and mixed into 5% dextrose solution (D), 0.9% isotonic NaCl solution and

phosphate buffer saline (PBS) solution separately (Table 1). These standard solutions were well-mixed and sonicated to obtain homogenous solutions for more accurate measurements. Thereafter, the solutions were incubated at 37 °C to mimic body temperature and analyzed over a three-week period to evaluate the delivery systems [25]. To imitate the gastrointestinal (GI) tract, various pH values and different compositions of fluids were chosen as parameters of this study.

Table 1. Solution concentrations (mg/mL) of samples for Zeta-sizer and UV/VIS measurements.

S	AMP	CEF	I	I-A	I-C	II	II-A	II-C	III	III-A	III-C
pH	0.12	0.003	0.3	0.012	0.003	0.003	0.3	0.003	0.03	0.12	0.006
5% D	0.12	0.003	0.3	0.012	0.003	0.003	0.3	0.003	0.03	0.12	0.006
PBS	0.12	0.003	0.3	0.012	0.003	0.003	0.3	0.003	0.03	0.12	0.006
0.9% NaCl	0.12	0.003	0.3	0.012	0.003	0.003	0.3	0.003	0.03	0.12	0.006

2.6. Sample Preparation for Antibacterial Tests

In order to prepare agar medium, 28 g of nutrient agar and 1 L of distilled water were mixed with a magnetic stirrer for 10 min until fully dissolved. This solution was autoclaved at 121 °C degrees for 15 min for sterilization. It was cooled down to 45 °C degrees and transferred into sterilized Petri dishes and allowed to solidify.

In order to prepare broth, 13 g of nutrient broth was dissolved in 1 L of distilled water. This solution was autoclaved at 121 °C degrees for 15 min for sterilization. The bacterial strains that were used in antibacterial activity tests were incubated in nutrient broth at 37 °C degrees for 48 h. The resulting bacterial culture was diluted with physiological saline solution and adjusted to 108 CFU/mL according to the McFarland 0.5 turbidity standard. In this study, both gram-positive (*Staphylococcus aureus*) and gram-negative (*Escherichia coli*) bacteria were utilized.

Anti-bacterial activities of the samples were tested by the agar disk diffusion method. An amount of 20 µL of bacterial suspensions (108 CFU/mL) that were prepared according to the 0.5 McFarland turbidity standard were taken and planted into previously prepared feed lots in Petri dishes. After that, 6 mm diameter wells were created. A total of 25 µL of solution where samples were dissolved in DMSO (8 mg/mL) with 200 µg of antibiotics was added to these wells and incubated at 37 °C degrees for 24 h.

3. Results

3.1. Characterization Part

3.1.1. Structural Characterization of PMVEMA-AMP DFMAC

FTIR/ATR and ^{1}H NMR analysis were used to characterize the synthesized drug-functionalized maleic anhydride copolymers and to provide detailed information and comparison based on chemical structure and functional groups. In Figure 2, comparative FTIR/ATR spectra of PMVEMA, AMP and PMVEMA-AMP are shown.

According to the FTIR/ATR spectrum of PMVEMA in Figure 2, peaks at ν = 1856 cm^{-1} (C=O stretching-anhydride), 1771 cm^{-1} (C=O stretching-cyclopentanone), 1218 cm^{-1} (-O-CH_3 stretching), 1078 cm^{-1} (O=C-O-C=O stretching-anhydride) and 920 cm^{-1} (-C-H bending) were observed.

The carbonyl group of the beta-lactam ring in vibration mode appeared around ν = 1770 cm^{-1} [26] as seen on the FTIR/ATR spectrum of AMP in Figure 2. Carbonyl group absorption for ampicillin trihydrate appeared around ν = 1769 cm^{-1}, and the peak for the side amide link on the beta-lactam ring appeared at ν = 1686 cm^{-1}. A very broad O-H group peak belonging to carboxylic acid was seen around ν = 2969 cm^{-1}.

According to the FTIR/ATR spectrum of PMVEMA-AMP in Figure 2, broad carboxylic acid at ν = 3225 cm^{-1} (O-H stretching), alkane at ν = 2978 cm^{-1} (CH_3 (a)symmetric stretching) and cyclobutane at ν = 2939 cm^{-1} (CH_2 symmetric stretching) were observed. Peaks at ν = 1763 cm^{-1} (C=O group of beta-lactam) and 1651 cm^{-1}, a carboxylic acid peak

at ν = 1704 cm^{-1} (C=O stretching), three substituted alkene peaks at ν = 1651 cm^{-1} (C=C str.), a 2° amide (of β-lactam) at ν = 1651 cm^{-1} (C=O stretching) and a monosubstituted benzene ν = 1497 cm^{-1} (C-C stretching) peak were also observed.

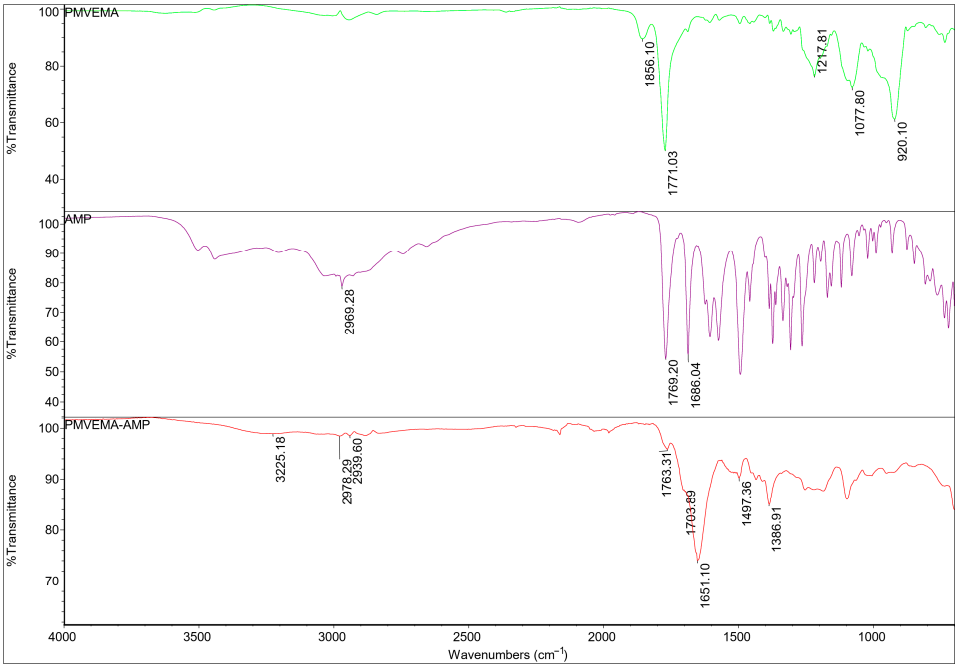


Figure 2. FTIR/ATR spectra of PMVEMA, AMP and PMVEMA-AMP.

In the reaction mechanism, the anhydride was exposed to a ring-opening reaction and anhydride peaks should have disappeared in the FTIR/ATR spectra. The conjugation of drug molecules with polymers led to new amide bond formation which can be observed in the spectra. The characteristic symmetric and asymmetric C=O stretching vibration peaks of anhydride of PMVEMA at 1856 and 1771 cm^{-1} disappeared. The carbonyl group peak of the beta-lactam ring of AMP was shifted from 1769 cm^{-1} to 1763 cm^{-1}. After the PMVEMA-AMP conjugation, new peaks at 1763 cm^{-1} (–N–C=O) and 1651 cm^{-1} (CO–N–H) due to amide formation are seen in Figure 2.

According to the ^{1}H NMR spectrum of PMVEMA-AMP in Figure S1a, ^{1}H NMR (400 MHz, dmso-d6) δ: 8.31 ppm (1H, N-H), 8.02 ppm (1H, N-H), 7.40–7.31 ppm (5H, C-H), 6.24 ppm (1H, C-H), 6.09 ppm (1H, C-H), 5.85 ppm (1H, C-H), 3.24 ppm (3H, CH_3), 3.05 ppm (1H, C-H), 2.93 ppm (1H, C-H), 2.34 ppm (1H, C-H), 1.98 ppm (1H, C-H), 1.92 ppm (6H, CH_3), 1.23 ppm (2H, CH_2).

3.1.2. Structural Characterization of PIBMA-AMP DFMAC

Comparative FTIR/ATR spectra of PIBMA, AMP and PIBMA-AMP are given in Figure 3.

According to the FTIR/ATR spectrum of PIBMA in Figure 3, peaks at ν = 1853 cm^{-1} (C=O stretching-anhydride), 1770 cm^{-1} (C=O stretching-cyclopentanone), 1474 cm^{-1} (C-H bending-dimethyl), 1219 cm^{-1} (-O-CH_3 stretching), 1075 cm^{-1} (O=C-O-C=O stretching-anhydride) and 909 cm^{-1} (-C-H bending) were observed.

According to the FTIR/ATR spectrum of PIBMA-AMP in Figure 3, broad carboxylic acid peaks at ν = 3284 cm^{-1} (O-H stretching), alkane at ν = 2967 cm^{-1} (CH_3 (a)symmetric stretching), cyclobutane at ν = 2933 cm^{-1} (CH_2 symmetric stretching), a beta-lactam ring peak at ν = 1778 cm^{-1} (C=O stretching), a carboxylic acid peak at ν = 1704 cm^{-1} (C=O stretching), three substituted alkene peaks at ν= 1649 cm^{-1} (C=C str.), a 2° amide (of β-lactam) at ν = 1649 cm^{-1} (C=O stretching) and monosubstituted benzene at ν= 1497 cm^{-1} (C-C stretching) were observed.

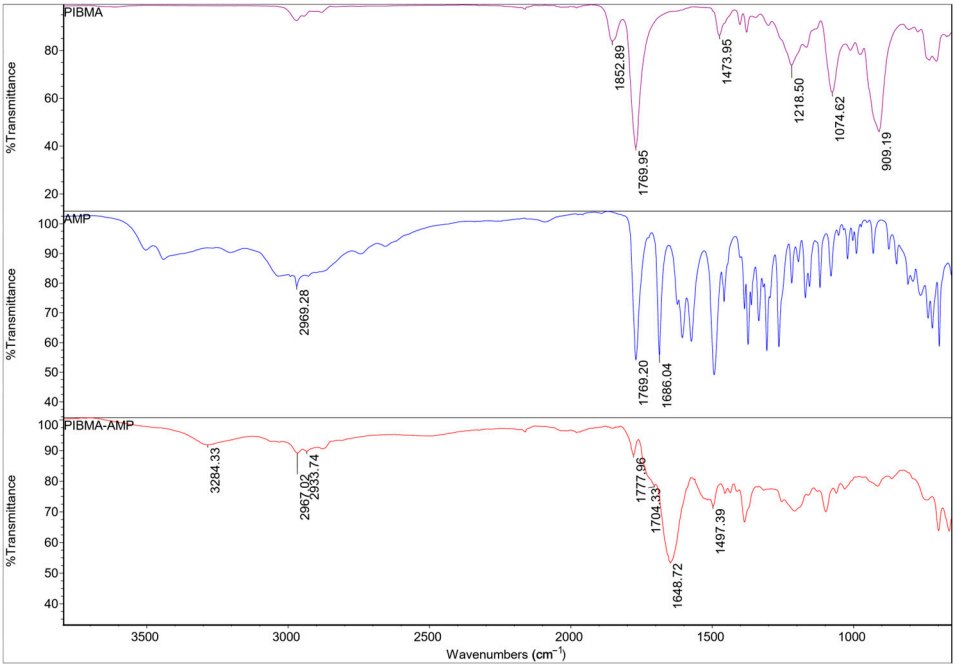


Figure 3. FTIR/ATR spectra of PIBMA, AMP and PIBMA-AMP.

The characteristic symmetric and asymmetric C=O stretching vibration peaks of anhydride of PIBMA at 1853 and 1770 cm^{-1} disappeared. The carbonyl group peak of the beta-lactam ring of AMP shifted from 1770 cm^{-1} to 1778 cm^{-1}. After the PIBMA-AMP conjugation, new peaks at 1778 cm^{-1} (–N–C=O) and 1649 cm^{-1} (CO–N–H) due to amide formation can be seen in Figure 3.

According to the ^{1}H NMR spectrum of PIBMA-AMP in Figure S1b, ^{1}H NMR (400 MHz, dmso-d6) δ: 8.26 ppm (1H, N-H), 7.99 ppm (1H, N-H), 7.30–7.26 ppm (5H, C-H), 5.64 ppm (1H, C-H), 4.86 ppm (1H, C-H), 4.56 ppm (1H, C-H), 3.02 ppm (1H, C-H), 2.97 ppm (1H, C-H), 2.65 ppm (1H, C-H), 1.49 ppm (1H, C-H), 1.12 ppm (6H, CH_3), 0.96 ppm (2H, CH_2).

3.1.3. Structural Characterization of PEMA-AMP DFMAC

The FTIR/ATR spectra of PEMA, AMP, PEMA-AMP comparatively are given in Figure 4.

According to the FTIR/ATR spectrum of PEMA in Figure 4, peaks at ν = 1849 cm^{-1} (C=O stretching-anhydride) and 1770 cm^{-1} (C=O stretching-cyclopentanone), 1218 cm^{-1} (-O-CH_3 stretching), 1094 cm^{-1} (O=C-O-C=O stretching-anhydride) and 915 cm^{-1} (-C-H bending) were observed.

According to the FTIR/ATR spectrum of PEMA-AMP in Figure 4, peaks at ν = 3287 cm^{-1} (O-H stretching of broad carboxylic acid), alkane at ν = 2980 cm^{-1} (CH_3 (a)symmetric stretching), peaks at ν = 1762 cm^{-1} (C=O group of beta-lactam), a carboxylic acid peak at ν = 1704 cm^{-1} (C=O stretching), three substituted alkene peaks at ν = 1649 cm^{-1} (C=C str.), a 2° amide (of β-lactam) at ν = 1649 cm^{-1} (C=O stretching), and monosubstituted benzene at ν = 1497 cm^{-1} (C-C stretching) were observed.

The characteristic symmetric and asymmetric C=O stretching vibration peaks of anhydride of PEMA at 1849 and 1770 cm^{-1} disappeared. The carbonyl group peak of the beta-lactam ring of AMP shifted from 1769 cm^{-1} to 1762 cm^{-1}. After the PEMA-AMP conjugation, new peaks at 1762 cm^{-1} (–N–C=O) and 1649 cm^{-1} (CO–N–H) due to amide formation were observed, as shown in Figure 4.

According to the ^{1}H NMR spectrum of PEMA-AMP in Figure S1c, ^{1}H NMR (400 MHz, dmso-d6) δ: 8.32 ppm (1H, N-H), 8.00 ppm (1H, N-H), 7.37–7.31 ppm (5H, C-H), 5.65 ppm (1H, C-H), 4.60 ppm (1H, C-H), 4.39 ppm (1H, C-H), 3.06 ppm (1H, C-H), 2.94 ppm (1H, C-H), 2.68 ppm (1H, C-H), 1.51 ppm (6H, CH_3), 1.33 ppm (1H, C-H), 1.23 ppm (2H, CH_2).

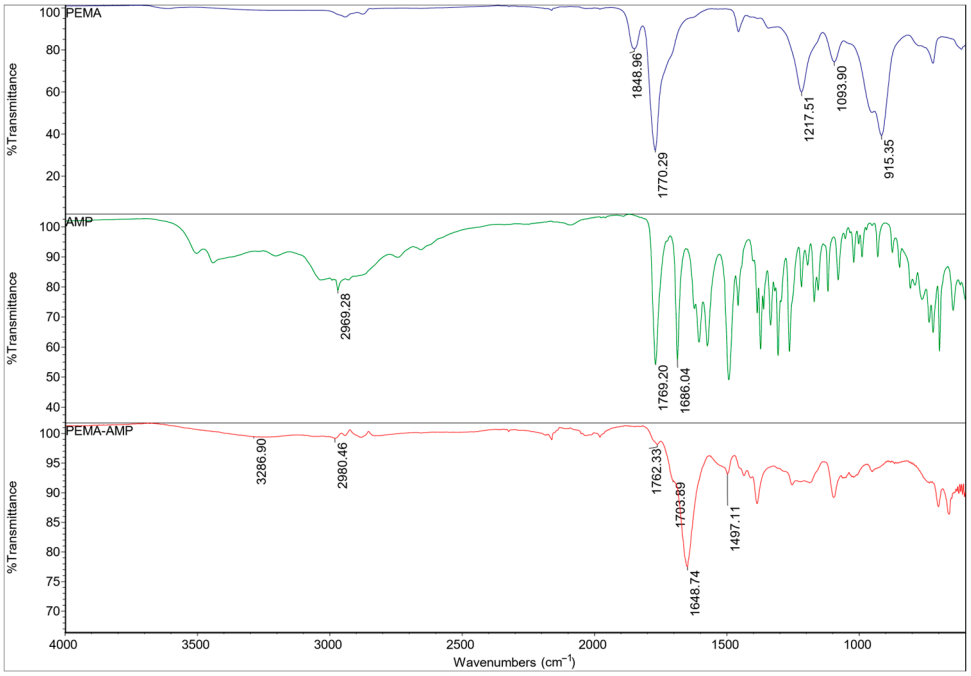


Figure 4. FTIR/ATR spectra of PEMA, AMP and PEMA-AMP.

3.1.4. Structural Characterization of PMVEMA-CEF DFMAC

The comparative FTIR/ATR spectra of PMVEMA, CEF and PMVEMA-CEF are given in Figure 5.

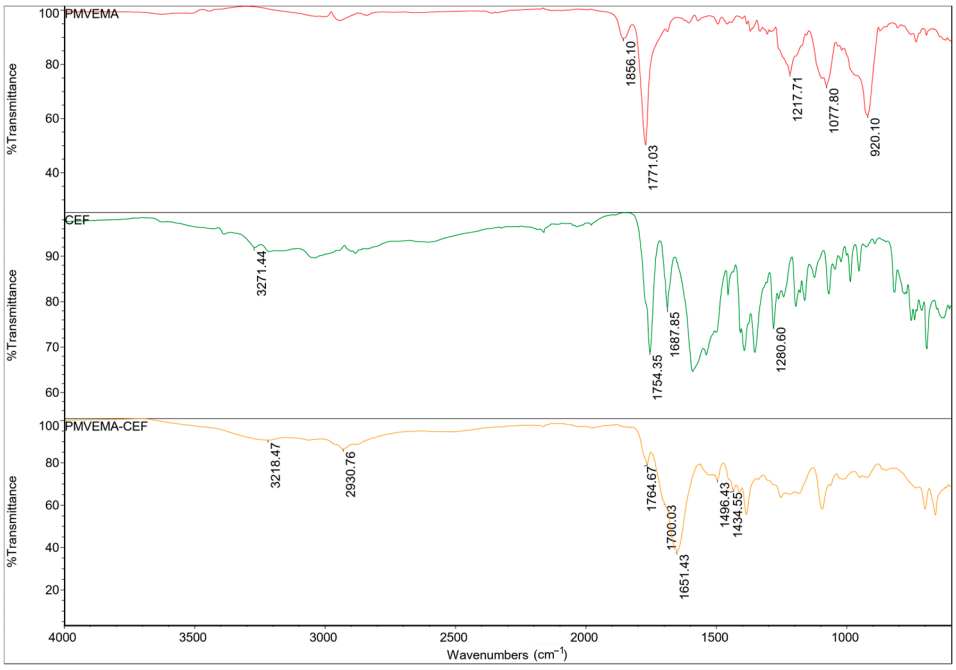


Figure 5. FTIR/ATR spectra of PMVEMA, CEF and PMVEMA-CEF.

Theoretically, the carbonyl group of the beta-lactam ring in vibration mode should appear around $\nu = 1770\ cm^{-1}$ [26]. As seen in the FTIR/ATR spectrum of CEF in Figure 5, carbonyl group absorption for cefalexin monohydrate appeared around $\nu = 1754\ cm^{-1}$ and the peak for the side amide link on the beta-lactam ring appeared at $\nu = 1688\ cm^{-1}$.

According to the FTIR/ATR spectrum of PMVEMA-CEF in Figure 5, peaks at $\nu = 3218\ cm^{-1}$ (O-H stretching of broad c. acid), alkane at $\nu = 2930\ cm^{-1}$ (CH_3 (a)symmetric stretch-

ing), peaks at ν = 1765 cm^{-1} (C=O group of beta-lactam), a carboxylic acid peak at ν = 1700 cm^{-1} (C=O stretching), three substituted alkene peaks at ν = 1651 cm^{-1} (C=C str.), a 2° amide (of β-lactam) at ν = 1651 cm^{-1} (C=O stretching) and monosubstituted benzene at ν = 1496 cm^{-1} (C-C stretching) were observed.

The characteristic symmetric and asymmetric C=O stretching vibration peaks of anhydride of PMVEMA at 1849 and 1770 cm^{-1} disappeared. The carbonyl group peak of the beta-lactam ring of CEF shifted from 1754 cm^{-1} to 1765 cm^{-1}. After the PMVEMA-CEF conjugation, new peaks at 1765 cm^{-1} (–N–C=O) and 1651 cm^{-1} (CO–N–H) due to amide formation can be seen in Figure 5.

According to the ^{1}H NMR spectrum of PMVEMA-CEF in Figure S1d, ^{1}H NMR (400 MHz, dmso-d6) δ: 8.65 ppm (1H, N-H), 8.13 ppm (1H, N-H), 7.39–7.33 ppm (5H, C-H), 4.98 ppm (1H, C-H), 4.79 ppm (1H, C-H), 4.41 ppm (1H, C-H), 3.37 ppm (3H, CH_3), 3.06 ppm (1H, C-H), 2.97 ppm (1H, C-H), 2.68 ppm (1H, C-H), 2.28 ppm (3H, CH_3), 1.00 ppm (2H, CH_2), 0.97 ppm (2H, CH_2).

3.1.5. Structural Characterization of PIBMA-CEF DFMAC

The comparative FTIR/ATR spectra of PIBMA, CEF and PIBMA-CEF are given in Figure 6.

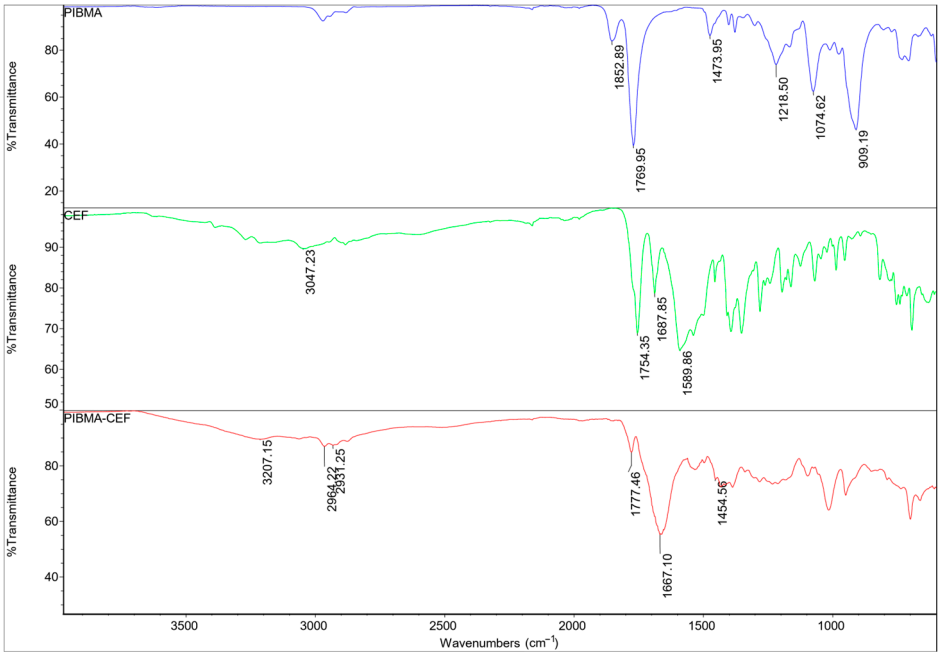


Figure 6. FTIR/ATR spectra of PIBMA, CEF and PIBMA-CEF.

In the FTIR/ATR spectrum of the PIBMA-CEF conjugate in Figure 6, broad carboxylic acid at ν = 3207 cm^{-1} (O-H stretching), alkane at ν = 2964 cm^{-1} (CH_3 (a)symmetric stretching), cyclobutane at ν = 2931 cm^{-1} (CH_2 symmetric stretching), a beta-lactam ring peak ν = 1777 cm^{-1} (C=O stretching), three substituted alkene peaks at ν = 1667 cm^{-1} (C=C str.), a 2° amide (of β-lactam) at ν = 1667 cm^{-1} (C=O stretching) and monosubstituted benzene ν = 1455 cm^{-1} (C-C stretching) were observed.

The characteristic symmetric and asymmetric C=O stretching vibration peaks of anhydride of PIBMA at 1853 and 1770 cm^{-1} disappeared. The carbonyl group peak of the beta-lactam ring of CEF shifted from 1754 cm^{-1} to 1778 cm^{-1}. After the PIBMA-CEF conjugation, new peaks at 1777 cm^{-1} (–N–C=O) and 1667 cm^{-1} (CO–N–H) due to amide formation can be seen in Figure 6.

In the ^{1}H NMR spectrum of PIBMA-CEF conjugate in Figure S1e, ^{1}H NMR (400 MHz, dmso-d6) δ: 8.69 ppm (1H, N-H), 8.45 ppm (1H, N-H), 7.41–7.33 ppm (5H, C-H), 4.96 ppm

(1H, C-H), 4.79 ppm (1H, C-H), 4.42 ppm (1H, C-H), 3.39 ppm (2H, CH_2), 3.06 ppm (1H, C-H), 2.97 ppm (1H, C-H), 1.31 ppm (3H, CH_3), 1.09 ppm (6H, CH_3), 0.99 ppm (2H, CH_2).

3.1.6. Structural Characterization of PEMA-CEF DFMAC

The FTIR/ATR spectra of PEMA, CEF and PEMA-CEF are given in Figure 7, comparatively.

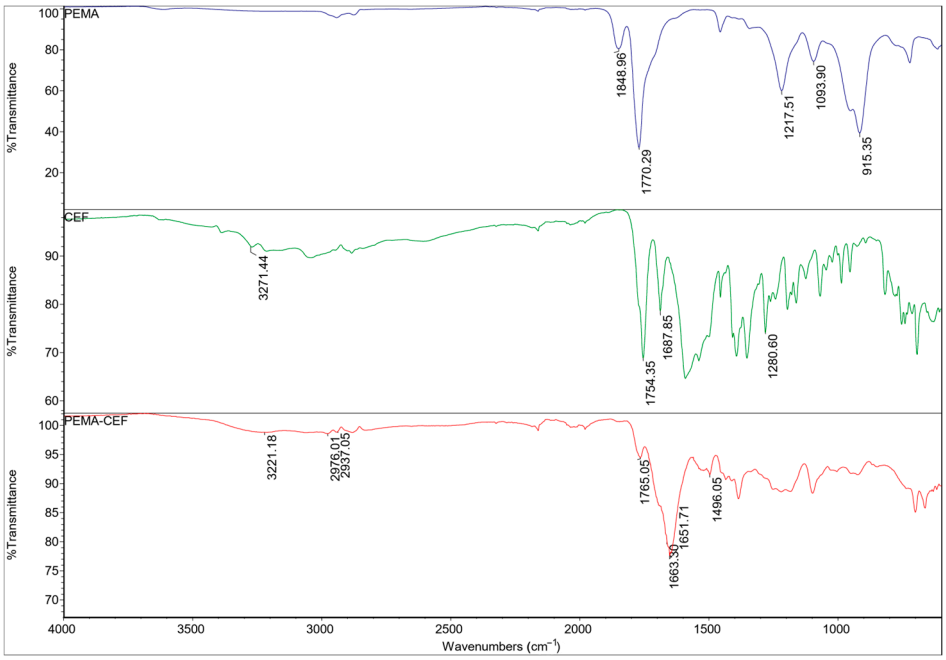


Figure 7. FTIR/ATR spectra of PEMA, CEF and PEMA-CEF.

In the FTIR/ATR spectrum of PEMA-CEF in Figure 7, broad carboxylic acid at ν = 3222 cm^{-1} (O-H stretching), alkane at ν = 2976 cm^{-1} (CH_3 (a)symmetric stretching), cyclobutene at ν = 2937 cm^{-1} (CH_2 symmetric stretching), a beta-lactam ring peak at ν= 1765 cm^{-1} (C=O stretching), three substituted alkene peaks at ν = 1652 cm^{-1} (C=C str.), a 2° amide (of β-lactam) at ν = 1663 cm^{-1} (C=O stretching) and monosubstituted benzene at ν = 1496 cm^{-1} (C-C stretching) were observed.

The characteristic symmetric and asymmetric C=O stretching vibration peaks of anhydride of PEMA at 1849 and 1770 cm^{-1} disappeared. The carbonyl group peak of the beta-lactam ring of CEF shifted from 1754 cm^{-1} to 1765 cm^{-1}. After the PEMA-CEF conjugation, new peaks at 1765 cm^{-1} (–N–C=O) and 1652 cm^{-1} (CO–N–H) due to amide formation were observed, as shown in Figure 7.

In the ^{1}H NMR spectrum of PEMA-CEF in Figure S1f, ^{1}H NMR (400 MHz, dmso-d6) δ: 8.64 ppm (1H, N-H), 8.43 ppm (1H, N-H), 7.39–7.33 ppm (5H, C-H), 5.01 ppm (1H, C-H), 4.78 ppm (1H, C-H), 4.43 ppm (1H, C-H), 3.06 ppm (1H, C-H), 2.97 ppm (1H, C-H), 2.31 ppm (2H, CH_2), 1.23 ppm (2H, CH_2), 1.16 ppm (3H, CH_3), 1.00 ppm (2H, CH_2).

3.2. Analysis Part

3.2.1. Comparative PDI, Particle Size and Stability Analyses of DFMACs at Different pH Values

The surface charge, zeta potential and pH of particles are crucial for understanding the state and stability of dispersions [27,28]. In Zeta-sizer measurements, the polydispersity index, particle size, mobility and zeta potential of drugs and DFMACs were monitored in terms of homogeneity, charge of the particles and stability.

The gastrointestinal tract (GI) spans from the stomach (pH 1.5–3.5) through the duodenum (pH 5–6) to the intestine (pH 7–8) [29,30]. Therefore, the drugs and DFMACs were evaluated across a broad pH scale.

The polydispersity index (PDI) defines the distribution of particle sizes in a population. A PDI 0.0 value indicates perfectly uniform particles (monodispersity) whereas a PDI 1.0 value indicates a range of particle sizes, namely, polydispersity [31]. PDI analyses are crucial for assessing the efficiency of the DFMACs. All drugs and DFMACs were evaluated in terms of PDI, particle size and stability analyses, respectively. In Table 2, polydispersity index (PDI) values of AMP, CEF and all DFMACs are shown with changing pH values.

Table 2. The PDI values of AMP, CEF and DFMACs particles at different pH values.

pH	AMP	CEF	PMVEMA-AMP	PIBMA-AMP	PEMA-AMP	PMVEMA-CEF	PIBMA-CEF	PEMA-CEF
2	0.32	0.34	0.39	0.11	0.35	0.33	0.31	0.30
3	0.34	0.35	0.38	0.30	0.32	0.33	0.33	0.34
4	0.30	0.32	0.29	0.28	0.33	0.33	0.33	0.30
5	0.31	0.33	0.34	0.26	0.33	0.35	0.36	0.30
6	0.67	0.37	0.35	0.29	0.32	0.37	0.35	0.37
7	0.33	0.41	0.33	0.30	0.30	0.35	0.33	0.32
8	0.31	0.34	0.36	0.24	0.44	0.45	0.32	0.36
9	0.33	0.60	0.37	0.31	0.36	0.42	0.34	0.32
10	0.31	0.36	0.39	0.31	0.38	0.36	0.33	0.36
11	0.31	0.36	0.34	0.31	0.34	0.33	0.35	0.37
12	0.33	0.32	0.33	0.32	0.42	0.35	0.31	0.67
13	0.34	0.32	0.34	0.36	0.36	0.39	0.34	0.46
Mean, SD	0.35 ± 0.10	0.37 ± 0.08	0.35 ± 0.03	0.28 ± 0.06	0.65 ± 0.04	0.36 ± 0.04	0.33 ± 0.02	0.37 ± 0.10
U	0.03	0.02	0.01	0.02	0.01	0.01	0.00	0.03

The polydispersity index belonging to DFMACs in solution should be as low as possible and the size distribution should be monodispersed [32]. Particles of all DFMACs were monodispersed in this pH range. Although all drugs and DFMACs were monodispersed, PIBMA-conjugated drugs exhibited lower PDI values than the others at different pH values. Hydrophobic group attachment leads to a slight decrease in PDI values [33]; likewise, the same effect was seen in PDI analysis. The distribution of particles was not significantly affected by the pH change.

Particle size affects the drug dissolution, absorption [34] and pharmacokinetics [31] in orally given solid drugs like AMP and CEF.

In Table 3, at both extremes of the studied pH range, the size of the particles of AMP and DFMACs increased and clustered. pH values between 5 and 8 gave the ideal particle size for AMP and DFMACs, in terms of aggregation. According to Table 3, CEF particles accumulated in the middle of the pH range, whereas particles of CEF conjugated maleic anhydride copolymers were dispersed in solution when their particle size was considered. All particles were of a sub-micro scale less than 1000 nm. Particle sizes between 1 and 1000 nm have special advantages in the oral administration of drugs [35]. According to Kamaly et.al.'s study [36], polymeric particles of sub-micro scale possess certain properties such as standardized fabrication, higher drug loading capacity, biodegradability and in vivo degradability.

The mobility values of AMP, CEF and all DFMACs with changing pH values are given in Table S1. All the particles of drugs and DFMACs were negatively charged across the whole pH range. The absolute mobility values of DFMACs were higher than those of AMP and CEF.

The stability of particle dispersion in a solution is assessed by zeta potential analysis. A value of zeta potential of ±10 mV indicates incipient stability [37] while a value greater than ±25 mV indicates a stable suspension [38]. The stability of dispersion is maintained by the electrostatic repulsion between the charged particles [38]. A higher value of zeta potential whether positive or negative indicates physically stable suspensions [39,40].

Table 3. The particle size values of AMP, CEF and DFMACs particles at different pH values.

pH	AMP	CEF	PMVEMA-AMP	PIBMA-AMP	PEMA-AMP	PMVEMA-CEF	PIBMA-CEF	PEMA-CEF
2	870	560	990	672	960	756	767	851
3	850	485	890	396	765	494	708	764
4	750	490	300	207	679	85	657	530
5	710	668	420	196	523	105	627	566
6	685	867	460	218	506	110	541	577
7	680	868	460	222	590	130	544	582
8	680	831	580	288	615	379	571	585
9	670	763	590	364	670	394	580	620
10	690	776	660	362	680	740	587	698
11	745	627	750	486	727	780	651	741
12	900	577	775	728	738	865	722	795
13	990	571	800	857	875	874	843	878
Mean, SD	768 ± 107	674 ± 142	640 ± 208	416 ± 224	694 ± 133	476 ± 318	650 ± 95	682 ± 121
U	31	41	60	65	38	92	27	35

In Table 4, the zeta potential values of DFMACs increased regardless of charge and showed greater stability in the middle of the pH range. However, drugs were significantly more stable in basic conditions. Absolute zeta potential values of all the particles of drugs shrank in the very low pH values and showed no stability. However, at the same pH values, the DFMACs had greater zeta potential values than the values of incipient stability. It is understood that absolute zeta potential values of AMP and CEF increased in acidic conditions by chemical conjugation with maleic anhydride copolymers and, as a result, drugs became stable in DFMAC form, especially with the PMVEMA conjugation.

Table 4. The zeta potential values (mV) of AMP, CEF and DFMACs at different pH values.

pH	AMP	CEF	PMVEMA-AMP	PIBMA-AMP	PEMA-AMP	PMVEMA-CEF	PIBMA-CEF	PEMA-CEF
2	−2.1	−4.8	−13.7	−10.9	−9.9	−14.1	−10.2	−11.9
3	−2.4	−8.5	−15.9	−11.9	−10.1	−14.6	−16.4	−13.4
4	−4.5	−18.9	−20.0	−17.8	−16.5	−14.9	−17.9	−14.9
5	−9.8	−19.4	−32.1	−25.2	−17.3	−24.3	−20.5	−17.2
6	−5.1	−19.7	−36.8	−25.2	−20.0	−22.7	−24.2	−20.9
7	−10.5	−16.2	−38.5	−22.9	−21.2	−22.4	−20.5	−22.4
8	−11.9	−16.7	−29.0	−22.8	−22.2	−22.3	−17.9	−21.9
9	−12.6	−21.2	−27.8	−15.6	−21.5	−21.2	−17.7	−19.7
10	−12.6	−20.1	−27.7	−23.8	−21.4	−19.4	−17.6	−18.2
11	−14.4	−21.9	−25.8	−21.4	−19.4	−19.2	−17.4	−16.2
12	−24.2	−18.2	−23.8	−16.7	−19.6	−17.7	−16.9	−12.3
13	−15.5	−16.0	−20.6	−14.9	−18.4	−14.8	−12.9	−10.8
Mean, SD	−10.5 ± 6.3	−16.8 ± 5.1	−26.0 ± 7.7	−19.1 ± 5.1	−18.1 ± 4.2	−19.0 ± 3.7	−17.5 ± 3.6	−16.7 ± 4.0
U	1.8	1.5	2.2	1.5	1.2	1.1	1.0	1.2

3.2.2. Temporal In Vitro Stability Tests of All DFMACs in Simulated Body Fluids

In oral drug delivery systems, a drug can pass through six different types of body fluids such as simulated gastric fluid, simulated intestinal fluid and simulated colonic fluid in a fasted-state/fed-state. The composition of those body fluids affects the possible in vivo behavior of a drug. Sodium chloride is present in fasted-state/fed-state simulated gastric fluid and fasted-state/fed-state simulated intestinal fluid. PBS (phosphate buffer saline) is used to mimic colonic fluid [41]. Additionally, 5% dextrose solution can stay in gastric fluid due to food intake in fed-state [42]. To understand the behavior of the orally administered drug in the gastrointestinal tract, different environmental solutions and various pH values

should be considered. Temporal in vitro stability tests should be conducted to understand the changing behavior of novel DFMACs over a three-week period.

The polydispersity index values of AMP, CEF and all DFMACs in 5% dextrose solution are given in Table 5.

Table 5. The PDI values of AMP, CEF and DFMACs in 5% dextrose solution.

Time (min)	AMP	CEF	PMVEMA-AMP	PIBMA-AMP	PEMA-AMP	PMVEMA-CEF	PIBMA-CEF	PEMA-CEF
0	0.28	0.43	0.34	0.35	0.42	0.39	0.37	0.35
15	0.28	0.61	0.32	0.34	0.53	0.35	0.34	0.33
30	0.27	0.39	0.33	0.33	0.39	0.38	0.33	0.36
60	0.27	0.38	0.35	0.34	0.37	0.36	0.38	0.36
120	0.27	0.43	0.33	0.33	0.37	0.39	0.39	0.43
180	0.27	0.47	0.42	0.34	0.36	0.39	0.32	0.36
1440 (1 d)	0.35	0.43	0.40	0.34	0.33	0.37	0.38	0.31
2880 (2 d)	0.34	0.33	0.38	0.34	0.36	0.37	0.37	0.33
4320 (3 d)	0.32	0.34	0.39	0.33	0.45	0.43	0.35	0.35
10,080 (1 w)	0.27	0.34	0.38	0.34	0.44	0.40	0.56	0.43
20,160 (2 w)	0.34	0.60	0.37	0.34	0.31	0.42	0.47	0.29
30,240 (3 w)	0.35	0.35	0.38	0.33	0.42	0.38	0.47	0.32
Mean, SD	0.30 ± 0.04	0.43 ± 0.10	0.37 ± 0.03	0.34 ± 0.01	0.40 ± 0.06	0.39 ± 0.02	0.39 ± 0.07	0.35 ± 0.04
U	0.01	0.03	0.01	0.00	0.02	0.01	0.02	0.01

According to Table 5, all particles of drugs and DFMACs were monodispersed. The homogeneity of particles of DFMACs was not much affected by time. The PDI values of AMP increased as time went by, due to the aggregation of particles. The average PDI value of CEF was significantly decreased by polymer conjugation.

Table 6 indicates that particles of AMP and CEF formed clusters within a day and Table S2 supports that drugs became immobile after the second day. On the other hand, DFMACs showed minimal aggregation at the end of the three-week period and particles exhibited higher mobility values in Table S2. The average particle size of DFMACs was smaller than that of pure drugs. Even after three weeks, all particles of DFMACs remained on the sub-micro scale. Since the stability of drugs increased by polymer conjugation, the formation of clusters was prevented and the size of the particles remained at a sub-micro scale over a three-week period.

Table 6. The particle size values (nm) of AMP, CEF and DFMACs particles in 5% dextrose solution.

Time (min)	AMP	CEF	PMVEMA-AMP	PIBMA-AMP	PEMA-AMP	PMVEMA-CEF	PIBMA-CEF	PEMA-CEF
0	550	773	345	300	603	542	333	678
15	570	783	365	330	620	558	340	621
30	515	921	385	335	626	607	356	611
60	520	1055	390	335	640	660	411	661
120	530	1038	435	335	647	692	534	627
180	530	1046	490	340	680	714	680	617
1440 (1 d)	590	1156	500	400	684	786	759	622
2880 (2d)	1010	1347	500	440	654	801	786	624
4320 (3 d)	1020	1371	525	515	703	843	793	633
10,080 (1 w)	1520	1396	550	495	784	850	905	645
20,160 (2 w)	1550	1379	590	465	792	852	906	674
30,240 (3 w)	1570	1469	610	440	853	864	949	748
Mean, SD	873 ± 444	1145 ± 246	474 ± 89	394 ± 74	691 ± 79	731 ± 119	646 ± 238	647 ± 39
U	128	71	26	21	23	34	69	11

In Table 7, zeta potential values regardless of sign showed a decreasing trend for drugs and DFMACs over time. AMP and CEF became unstable after the first day and the stability of DFMACs extended up to three weeks. Notably, PMVEMA and PEMA conjugated drugs had higher absolute zeta potential values and better stability as also shown in Figure 8.

Table 7. The zeta potential values (mV) of AMP, CEF and DFMACs in 5% dextrose solution.

Time (min)	AMP	CEF	PMVEMA-AMP	PIBMA-AMP	PEMA-AMP	PMVEMA-CEF	PIBMA-CEF	PEMA-CEF
0	−30.5	−7.9	−28.2	−27.2	−24.5	−19.0	−18.7	−23.6
15	−26.6	−9.8	−28.0	−22.0	−24.0	−18.8	−17.4	−23.3
30	−26.2	−10.6	−24.8	−21.4	−23.7	−18.3	−16	−22.4
60	−24.4	−8.3	−24.3	−19.0	−22.8	−18.6	−15.4	−26.3
120	−23.4	−12.2	−21.9	−19.2	−22.6	−19.6	−14.8	−23.2
180	−22.8	−14.3	−20.8	−19.1	−22.5	−20.3	−13.7	−20.9
1440 (1 d)	−22.5	−10.6	−21.7	−19.6	−21.5	−19.4	−12.3	−20.9
2880 (2 d)	−11.3	−9.9	−21.2	−18.7	−20.3	−17.6	−11.9	−19.1
4320 (3 d)	−7.5	−6.1	−21.1	−17.4	−20.9	−16.3	−10.9	−17.9
10,080 (1 w)	−3.6	−3.2	−19.4	−12.7	−18.6	−15.8	−10.7	−16.2
20,160 (2 w)	−3.3	−2.7	−18.0	−10.5	−15.3	−14.0	−10.4	−15.4
30,240 (3 w)	−3.1	−2.5	−17.6	−9.2	−15.4	−14.1	−9.1	−14.3
Mean, SD	−17.1 ± 10.5	−8.2 ± 3.8	−22.3 ± 3.5	−18.0 ± 5.1	−21.0 ± 3.1	−17.7 ± 2.1	−13.4 ± 3.0	−20.3 ± 3.7
U	3.0	1.1	1.0	1.5	0.9	0.6	0.9	1.1

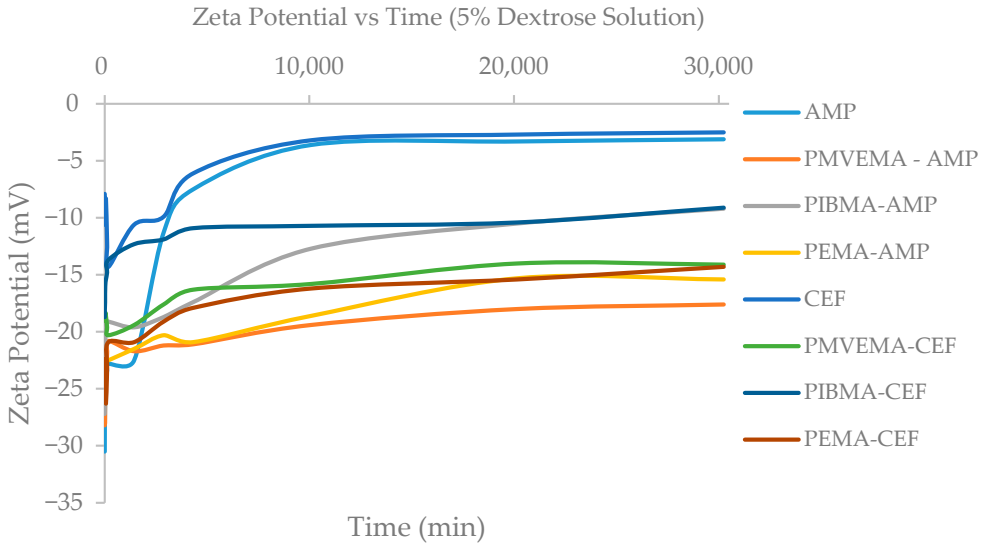


Figure 8. Zeta potential (mV) vs. time (min) in 5% dextrose.

An overall decreasing trend in zeta potential can be seen in Figure 8, and DFMACs exhibit higher absolute zeta potential values than drugs. The absolute zeta potential values of drugs drastically decreased after a week, whereas DFMACs exhibited a smoother decline.

According to Table 8, all particles were monodispersed and homogenously dispersed in the sample solutions. Similar to basic conditions, conjugation did not significantly affect the PDI values of drugs. All the particles were negatively charged (as shown in Table S3). There was a stronger interaction between particles of the drugs than between the particles of the DFMAC solution in basic PBS solution. The presence of protonated drug molecules in DFMAC solutions reduced the repulsive forces.

Table 8. The PDI values of AMP, CEF and all DFMACs in the PBS solution.

Time (min)	AMP	CEF	PMVEMA-AMP	PIBMA-AMP	PEMA-AMP	PMVEMA-CEF	PIBMA-CEF	PEMA-CEF
0	0.32	0.37	0.40	0.38	0.33	0.35	0.41	0.34
15	0.36	0.31	0.45	0.47	0.45	0.33	0.38	0.30
30	0.43	0.33	0.43	0.33	0.36	0.36	0.57	0.38
60	0.32	0.30	0.36	0.31	0.37	0.33	0.42	0.36
120	0.31	0.34	0.37	0.32	0.39	0.38	0.35	0.31
180	0.35	0.37	0.33	0.34	0.36	0.39	0.34	0.39
1440 (1 d)	0.32	0.32	0.39	0.37	0.41	0.34	0.35	0.35
2880 (2 d)	0.29	0.38	0.53	0.33	0.36	0.29	0.35	0.36
4320 (3 d)	0.33	0.34	0.43	0.32	0.42	0.37	0.41	0.35
10,080 (1 w)	0.39	0.28	0.33	0.32	0.33	0.34	0.42	0.26
20,160 (2 w)	0.32	0.33	0.43	0.36	0.33	0.34	0.39	0.27
30,240 (3 w)	0.33	0.30	0.36	0.31	0.29	0.43	0.41	0.24
Mean, SD	0.34 ± 0.04	0.33 ± 0.03	0.40 ± 0.06	0.35 ± 0.05	0.37 ± 0.04	0.35 ± 0.04	0.40 ± 0.06	0.33 ± 0.05
U	0.01	0.01	0.02	0.01	0.01	0.01	0.02	0.01

Table 9 indicates that DFMACs exhibited cluster formation at the end of the three weeks, due to the increase in their particle size. However, clusters of particles of AMP and CEF led to some precipitation, causing the particle sizes of the drug solutions to become smaller after 3 days. The chemical composition of the solution affected the particle size of the drugs and DFMACs.

Table 9. The particle size values (nm) of AMP, CEF and all DFMACs in PBS solution.

Time (min)	AMP	CEF	PMVEMA-AMP	PIBMA-AMP	PEMA-AMP	PMVEMA-CEF	PIBMA-CEF	PEMA-CEF
0	610	785	683	789	742	689	643	700
15	640	850	688	837	754	699	691	712
30	790	862	746	970	773	748	650	713
60	810	811	756	868	783	823	733	734
120	825	832	758	860	795	851	765	725
180	840	806	778	866	797	876	736	736
1440 (1 d)	860	830	833	701	806	904	785	735
2880 (2 d)	840	819	845	711	868	913	793	738
4320 (3 d)	800	862	916	703	881	910	852	738
10,080 (1 w)	765	890	925	825	905	915	894	744
20,160 (2 w)	740	789	932	945	918	945	892	780
30,240 (3 w)	725	553	963	992	957	952	977	785
Mean, SD	770 ± 79	807 ± 86	819 ± 98	839 ± 100	832 ± 71	852 ± 93	784 ± 103	737 ± 25
U	23	25	28	29	20	27	30	7

In Table 10, the zeta potential values of drug and DFMACs, regardless of sign, showed a decreasing trend over a three-week period. AMP and CEF became unstable after the third day and the second week, respectively. Very low absolute zeta potential values of the drug were being compensated by copolymer conjugation. Absolute zeta potential values of all DFMACs showed stability over the three-week period.

In Figure 9, PMVEMA and PEMA conjugated drugs exhibited higher absolute zeta potential values and better stability than drug-functionalized PIBMA copolymers. Free drugs exhibited the lowest absolute zeta potential values.

According to Table 11, all particles of DFMACs in sample solutions were monodispersed. Over the three-week period, almost all of the DFMACs exhibited lower PDI values on average compared to antibiotics. In 0.9% NaCl solution, particles of DFMACs exhib-

ited more homogenous distribution than the particles of drugs. Ensuring homogenous distribution is crucial for the efficiency, stability and safety of drugs [31].

Table 10. The zeta potential values (mV) of drugs and all DFMACs in PBS solution.

Time (min)	AMP	CEF	PMVEMA-AMP	PIBMA-AMP	PEMA-AMP	PMVEMA-CEF	PIBMA-CEF	PEMA-CEF
0	−14.8	−13.4	−31.3	−16.8	−32.5	−30.4	−22.1	−23.3
15	−14.8	−15.2	−27.1	−20.3	−32.7	−27.5	−18.9	−22.2
30	−15.8	−14.7	−23.0	−19.7	−29.4	−25.6	−18.6	−21.3
60	−15.5	−14.9	−22.7	−18.6	−27.2	−23.4	−19.1	−18.3
120	−18.3	−13.1	−21.2	−14.0	−26.3	−24.4	−18.8	−17.1
180	−18.7	−14.5	−19.5	−14.0	−26.6	−24.0	−18.0	−17.1
1440 (1 d)	−14.8	−14.7	−18.6	−14.4	−26.3	−23.7	−17.2	−16.1
2880 (2 d)	−12.7	−13.4	−18.0	−13.7	−25.3	−23.2	−15.8	−16.0
4320 (3 d)	−13.9	−10.9	−17.7	−13.8	−22.7	−22.9	−15.6	−15.5
10,080 (1 w)	−8.3	−10.2	−15.6	−13.6	−22.5	−20.1	−15.3	−15.8
20,160 (2 w)	−7.5	−10.1	−15.4	−12.6	−22.2	−18.9	−14.1	−14.9
30,240 (3 w)	−8.0	−9.6	−14.5	−12.5	−20.5	−18.4	−13.8	−14.6
Mean, SD	−13.6 ± 3.8	−12.9 ± 2.1	−20.4 ± 5.0	−15.3 ± 2.8	−26.2 ± 3.9	−23.5 ± 3.4	−17.3 ± 2.4	−17.7 ± 3.0
U	1.1	0.6	1.4	0.8	1.1	1.0	0.7	0.9

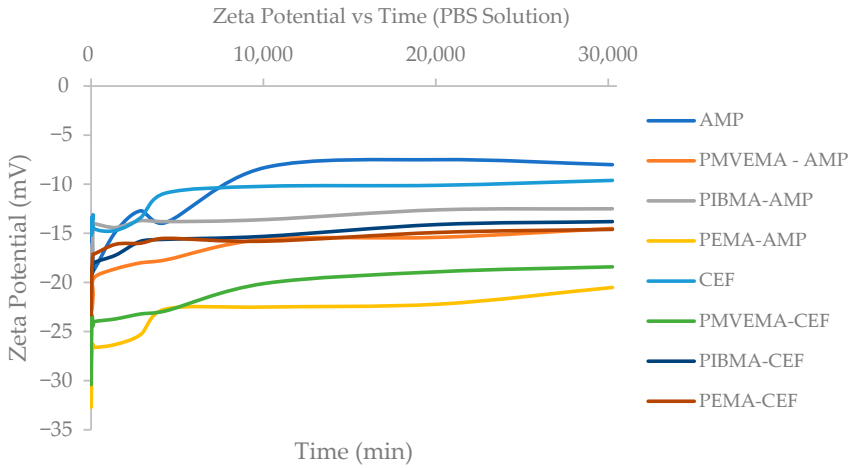


Figure 9. Zeta potential (mV) vs. time (min) in PBS solution.

Table 11. The PDI values of drugs and all DFMACs in 0.9% NaCl solution.

Time (min)	AMP	CEF	PMVEMA-AMP	PIBMA-AMP	PEMA-AMP	PMVEMA-CEF	PIBMA-CEF	PEMA-CEF
0	0.52	0.47	0.26	0.18	0.45	0.22	0.31	0.34
15	0.35	0.34	0.23	0.20	0.34	0.26	0.32	0.34
30	0.35	0.31	0.28	0.18	0.33	0.27	0.31	0.35
60	0.35	0.32	0.30	0.25	0.31	0.24	0.29	0.33
120	0.35	0.32	0.29	0.21	0.33	0.19	0.35	0.35
180	0.31	0.32	0.29	0.22	0.36	0.29	0.33	0.35
1440 (1 d)	0.57	0.37	0.37	0.23	0.33	0.26	0.34	0.51
2880 (2 d)	1.10	0.32	0.30	0.23	0.39	0.31	0.33	0.39
4320 (3 d)	0.77	0.34	0.35	0.24	0.38	0.35	0.32	0.59
10,080 (1 w)	0.43	0.32	0.36	0.32	0.32	0.38	0.35	0.35
20,160 (2 w)	0.33	0.34	0.34	0.42	0.13	0.38	0.30	0.34
30,240 (3 w)	0.33	0.32	0.35	0.33	0.40	0.35	0.34	0.41
Mean, SD	0.48 ± 0.24	0.34 ± 0.04	0.31 ± 0.04	0.25 ± 0.07	0.34 ± 0.08	0.29 ± 0.06	0.32 ± 0.02	0.39 ± 0.08
U	0.07	0.01	0.01	0.02	0.02	0.02	0.01	0.02

Table 12 indicates that particles of drugs and DFMACs formed clusters at the end of the three-week period. Clusters of particles of AMP aggregated and precipitated and the size of the particles became smaller after the first week, supported by the low mobility values in Table S4. On the other hand, CEF and DFMACs did not precipitate in the three-week period, but formed clusters. The small particle size results in the high absolute mobility values as demonstrated by Table 12 and Table S4.

Table 12. The particle size values (nm) of AMP, CEF and all DFMACs particles in 0.9% NaCl solution.

Time (min)	AMP	CEF	PMVEMA-AMP	PIBMA-AMP	PEMA-AMP	PMVEMA-CEF	PIBMA-CEF	PEMA-CEF
0	520	351	281	313	545	153	357	624
15	555	422	285	295	550	180	363	625
30	545	502	293	300	551	189	383	659
60	582	507	316	357	553	207	419	636
120	561	517	320	336	575	245	483	768
180	550	519	332	347	582	247	487	782
1440 (1 d)	528	526	338	341	593	261	502	796
2880 (2 d)	591	535	341	372	622	281	512	826
4320 (3 d)	570	611	357	392	656	326	531	912
10,080 (1 w)	855	616	518	715	668	714	647	917
20,160 (2 w)	846	653	703	830	709	728	695	923
30,240 (3 w)	748	660	746	887	856	738	719	962
Mean, SD	621 ± 122	535 ± 91	403 ± 163	457 ± 218	622 ± 91	356 ± 229	508 ± 124	786 ± 126
U	35	26	47	63	26	66	36	36

In Table 13, zeta potential values of all particles, regardless of sign, showed a decreasing trend in general. Very low zeta potential values of the drug were compensated and stabilized by copolymer conjugation, especially after the second day. PMVEMA and PEMA conjugation increased the zeta potential values and the stability significantly.

Table 13. The zeta potential values (mV) of AMP, CEF and DFMACs in 0.9% NaCl solution.

Time (min)	AMP	CEF	PMVEMA-AMP	PIBMA-AMP	PEMA-AMP	PMVEMA-CEF	PIBMA-CEF	PEMA-CEF
0	−9.6	−16.9	−25.6	−15.6	−27.1	−31.9	−22.4	−26.9
15	−10.1	−16.7	−25.3	−14.4	−25.3	−30.2	−19.2	−23.8
30	−15.1	−15.0	−23.6	−17.9	−25.1	−30.3	−17.9	−24.4
60	−15.4	−10.5	−23.1	−18.3	−24.1	−27.6	−17.0	−20.7
120	−14.9	−10.5	−21.7	−20.3	−23.3	−24.6	−17.9	−19.4
180	−14.1	−9.9	−21.2	−15.0	−22.9	−25.0	−18.4	−17.3
1440 (1 d)	−10.6	−9.0	−21.0	−14.1	−22.1	−24.0	−19.0	−16.9
2880 (2 d)	−9.5	−9.3	−20.1	−12.4	−21.3	−23.9	−19.1	−15.3
4320 (3 d)	−9.6	−9.1	−19.2	−10.1	−20.3	−23.4	−17.3	−15.4
10,080 (1 w)	−9.8	−9.6	−17.7	−11.3	−19.8	−23.9	−16.5	−14.4
20,160 (2 w)	−8.2	−8.4	−15.8	−10.8	−18.3	−21.7	−16.2	−13.8
30,240 (3 w)	−6.6	−8.0	−10.9	−10.1	−16.9	−20.9	−16.1	−13.7
Mean, SD	−11.1 ± 3.0	−11.1 ± 3.2	−20.4 ± 4.2	−14.2 ± 3.4	−22.2 ± 3.0	−25.6 ± 3.6	−18.1 ± 1.8	−18.5 ± 4.5
U	0.9	0.9	1.2	1.0	0.9	1.0	0.5	1.3

In Figure 10, it was evident that drugs have the lowest absolute zeta potential values overall. The absolute zeta potential values of all samples decreased with time.

Hence, all DFMACs in this research were analyzed considering time and pH change in various simulated body fluids such as 5% dextrose solution, phosphate-buffered saline (PBS) solution and 0.9% NaCl solution. Among the tested body fluids, 5% dextrose solution

and 0.9% isotonic NaCl solution led to more stable results for DFMACs compared to PBS solution due to the basicity of this solution.

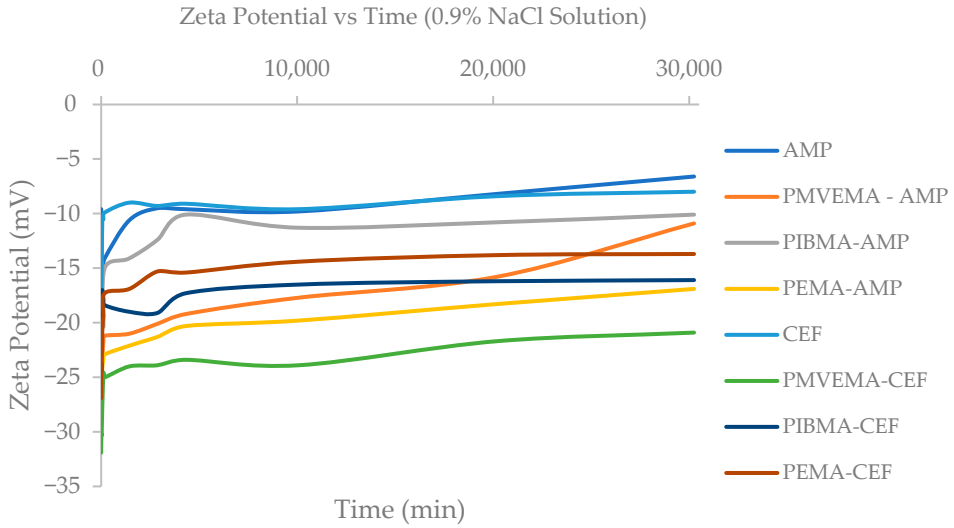


Figure 10. Zeta potential (mV) vs. time (min) in 0.9% NaCl solution.

Since the pH value and the chemical composition of the medium imitate the GI, the order of the GI from stomach to colon is crucial. The drugs and DFMACs were first exposed to a highly acidic medium with 0.9% isotonic NaCl solution, simulating conditions similar to the stomach, and subsequently to a basic pH environment with PBS solution, resembling conditions found in the colon. In this order, drugs and DFMACs should be stable, active, monodispersed and mobile, as long as possible to be efficient. However, drugs were active in acidic conditions, but unstable in acidic conditions and susceptible to dissolution in gastric media.

On the other hand, DFMACs met the requirements by demonstrating prolonged stability, activity and mobility, making them efficient alternatives to those drugs.

3.2.3. Activity Analysis of AMP, CEF and DFMACs at Different pH Values and in Simulated Body Fluids

pH-dependent and time-dependent changes in the activity of drugs and DFMACs were assessed by using UV/VIS spectroscopy. The UV/VIS spectra are shown in Figures S2–S9. The pH values and time points at which AMP, CEF and DFMACs exhibited maximum activity in simulated body fluids are summarized in Table 14.

Table 14. The pH values and time points at which AMP, CEF and DFMACs exhibited maximum activity.

Sample	pH	5% Dex	PBS	0.9% NaCl
AMP	6	1st week	2nd week	3rd week
PMVEMA-AMP	5	3rd week	2nd week	2nd week
PIBMA-AMP	2	2nd day	1st week	2nd day
PEMA-AMP	6	2 h	3rd week	3rd week
CEF	6	2nd day	1st week	1st week
PMVEMA-CEF	2	0 min	2nd week	3rd week
PIBMA-CEF	2	2nd day	2nd week	3rd week
PEMA-CEF	5	1st week	1st week	2 h

AMP and CEF antibiotics showed maximum activity mostly in the first week and after, whereas, according to zeta potential values, they had already became unstable within a week. Additionally, since they were eliminated from the body within a couple of hours [22], the activity profile of drugs was not in harmony with the stability and half-life of the drug. Drugs were more active at pH 6 and unstable in the very acidic gastric medium which is

the first part of the GI tract. Before reaching a higher pH medium, it would be exposed to decomposition in acid.

Comparatively, DFMACs exhibited high activity profiles in very low pH values like those of a gastric medium. DFMACs were also stable in the acidic medium which prevents the decomposition of DFMACs. In the simulated body fluids that mimic the GI tract, DFMACs maintained stability under maximum activity conditions.

3.2.4. Antibacterial Susceptibility Test Results

The disk diffusion method is distinguished by its simplicity, low cost, ability to test an excessive number of microorganisms and ease of result interpretation [43]. This method is especially suitable for fastidious bacterial pathogens [43] and serves as the indicator of the antibacterial activity of samples. Hence, in order to evaluate the antimicrobial effect of DFMACs, this method was used. According to CLSI (Clinical and Laboratory Standards Institute), diameters of inhibition zones for sensitive antimicrobials (S) are accepted as greater or equal to 20 mm, for intermediate antimicrobials (I) as between 15 and 19 mm and for resistant antimicrobials (R) as less or equal to 14 mm [44]. Intermediate antimicrobials inhibit the selected bacteria, and their inhibition zone can easily be widened by an increase in the concentration of antibacterials [44]. In Figure 11, DMSO was a blank control group for gram-positive and gram-negative bacteria. All maleic anhydride copolymers, pure antibiotics and DFMACs were tested against *S. aureus* gram-positive and *E. coli* gram-negative bacteria.

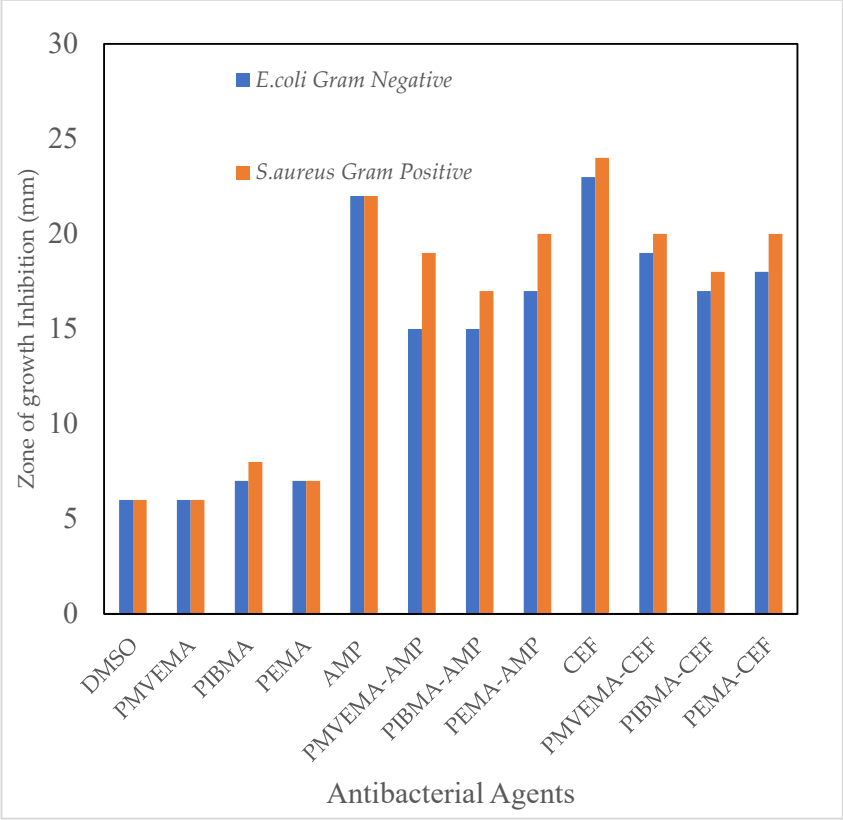


Figure 11. Inhibition zones of samples against gram-positive and gram-negative bacteria.

Since DMSO was a blank control group, it showed only the radius of the wells (6 mm). Maleic anhydride copolymers exhibited very little inhibition zones against the selected bacteria. All the DFMACs inhibited gram-positive and gram-negative bacteria, but they were more effective on gram-positive bacteria than gram-negative bacteria.

Cefalexin monohydrate is a hydrophobic compound, so it was retained by gram-negative and more effective on gram-positive bacteria whereas ampicillin trihydrate is

moderately hydrophilic and less effective on gram-positive bacteria than cefalexin monohydrate. This affected the antibacterial activity of DFMACs on gram-positive bacteria. All of the DFMACs introduced in this study inhibited the growth of gram-negative (*E. coli*) and gram-positive (*S. aureus*) bacteria like pure antibiotics. The inhibition zones of DFMACs can be enhanced [44] by increasing the drug to polymer ratio (Table S5). The aim of the antibacterial study was to show that the polymers gain antibacterial properties after drug functionalization. This analysis proved the efficacy of the DFMACs on certain bacterial groups, alongside the enhancement of pharmacological properties of free antibiotics by DFMACs.

4. Discussion

In this study, drug-functionalized maleic anhydride copolymers based on ampicillin trihydrate and cephalexin monohydrate were synthesized for the first time by a chemical conjugation method. Chemical characterization of polymer–antibiotic conjugates was conducted by ^{1}H NMR and FTIR/ATR spectroscopies. These conjugates at different pH values with simulated body fluids over specified time intervals were analyzed, utilizing zeta and UV/VIS spectroscopic measurements. Parameters such as pH values, time duration and composition of solutions affected the absorbance of samples.

The size of the particles of drug-functionalized maleic anhydride copolymers were on a sub-micro scale which has distinct benefits for administering drugs orally [35]. However, the particles of drugs became micro-sized in temporal and pH-dependent changes due to the aggregation of clusters among the particles. By the copolymer conjugation of antibiotics, the activity of drugs was extended over a longer time. DFMACs were stable in an extended pH range compared to the pure drugs. In general, DFMACs were more stable in the pH 2–6 band whereas drugs were unstable in acidic conditions and exposed to dissolution in gastric media. The activity and stability profiles of drugs were not aligned. On the other hand, DFMACs were stable when they exhibited a high activity profile. DFMACs demonstrated prolonged stability, activity and mobility and became efficient alternatives to the chosen drugs. Antibacterial tests proved that maleic anhydride copolymers acquired the bactericidal effect through antibiotic conjugation. The importance of antibacterial studies lay in the continuity of the antibacterial effect of drugs while enhancing pharmacokinetics through copolymer conjugation.

The stability ranking of synthesized DFMACs were as follows: PMVEMA-AMP > PEMA-AMP > PIBMA-AMP and PMVEMA-CEF > PEMA-CEF > PIBMA-CEF. The hydrophilicity of the polymer significantly influenced the stability of DFMACs, with more hydrophilic polymers providing greater stability. Additionally, the PMVEMA was considered as highly reactive to primary amines and facilitates the formation of amide more rapidly [45] than the other copolymers. Hence, PMVEMA-AMP and PMVEMA-CEF were observed as the most stable drug-functionalized maleic anhydride copolymers.

Regarding stability, activity and antibacterial efficiency, among the six different DFMACs studied, the most effective DFMACs overall were PMVEMA-conjugated drugs. The results demonstrated that the method of conjugation of the drug via an amide bond resulted in an improved macromolecular conjugate form, thereby improving the pharmacokinetics of the pharmacologically active substance. These DFMACs, chosen for two beta-lactam group antibiotics, exhibited better pharmacological properties and antibacterial activity compared to those found in the existing literature [46,47]. As a result, it can be concluded that the developed PMVEMA-CEF and PMVEMA-AMP are promising drug delivery system candidates alternative to AMP and CEF in the treatment of microbial infections. Given the successful polymer conjugation with both AMP and CEF from different sub-groups of the β-lactam family, this methodology holds potential for application across the entire β-lactam group. The results suggested promising prospects for using these macromolecular conjugates in pharmaceutical technology, potentially as implants.

Supplementary Materials: The following supporting information can be downloaded at: https://www.mdpi.com/article/10.3390/app14146112/s1, Figure S1: NMR spectra of PMVEMA-AMP (a), PIBMA-AMP (b), PEMA-AMP (c), PMVEMA-CEF (d), PIBMA-CEF (e) and PEMA-CEF (f). Figure S2: Absorption spectra of AMP (a), PMVEMA-AMP (b), PIBMA-AMP (c) and PEMA-AMP (d) at different pH values. Figure S3: Absorption spectra of CEF (a), PMVEMA-CEF (b), PIBMA-CEF (c) and PEMA-CEF (d) at different pH values. Figure S4: Absorption spectra of AMP (a), PMVEMA-AMP (b), PIBMA-AMP (c) and PEMA-AMP (d) in 5% dextrose solution. Figure S5: Absorption spectra of CEF(a), PMVEMA-CEF (b), PIBMA-CEF (c) and PEMA-CEF (d) in 5% dextrose solution. Figure S6: Absorption spectra of AMP (a), PMVEMA-AMP (b), PIBMA-AMP (c) and PEMA-AMP (d) in PBS solution. Figure S7: Absorption spectra of CEF (a), PMVEMA-CEF (b), PIBMA-CEF (c) and PEMA-CEF (d) in PBS solution. Figure S8: Absorption spectra of AMP (a), PMVEMA-AMP (b), PIBMA-AMP (c) and PEMA-AMP (d) in 0.9% NaCl solution. Figure S9: Absorption spectra of CEF (a), PMVEMA-CEF (b), PIBMA-CEF (c) and PEMA-CEF (d) in 0.9% NaCl solution. Table S1: The mobility values of AMP, CEF and all drug-functionalized maleic anhydride copolymers at different pH values. Table S2: The mobility values of AMP, CEF and all drug-functionalized maleic anhydride copolymers in 5% dextrose solution. Table S3: The mobility values of AMP CEF and all drug-functionalized maleic anhydride copolymers in PBS solution. Table S4: The mobility values of AMP, CEF and all drug-functionalized maleic anhydride copolymers in 0.9% NaCl solution. Table S5: Percentage of drug binding to copolymers, values belonging to copolymers and DFMACs.

Author Contributions: Conceptualization, D.S. and A.K.; methodology, D.S. and M.A.Y.; software, D.S. and A.K.; validation, D.S. and M.A.Y.; formal analysis, D.S. and A.K.; resources, D.S. and M.A.Y.; data curation, D.S., A.K. and M.A.Y.; writing—original draft preparation, D.S. and A.K.; writing—review and editing, D.S. and A.K.; visualization, A.K.; supervision, D.S.; project administration, D.S.; funding acquisition, D.S. and A.K. All authors have read and agreed to the published version of the manuscript.

Funding: This research received no external funding.

Institutional Review Board Statement: Not applicable.

Informed Consent Statement: Not applicable.

Data Availability Statement: The original contributions presented in the study are included in the article/supplementary material, further inquiries can be directed to the corresponding author.

Acknowledgments: The authors dedicated this publication to the 100th Anniversary of the Founding of the Modern Republic of Türkiye. We would like to thank to The Turkish Council of Higher Education "YOK" for the support within the scope of the YOK 100/2000 scholarship program specialized in micro- and nanotechnology. We would like to thank BILIM Pharmaceuticals for the drug supply.

Conflicts of Interest: The authors declare no conflicts of interest.

References

1. Bhattacharya, P.; Dutta, S.; Chandra, K.; Basak, A. The Never-Ending Story of β-Lactams: Use as Molecular Scaffolds and Building Blocks. In *Beta-Lactams: Novel Synthetic Pathways and Applications*; Banik, B.K., Ed.; Springer International Publishing: Cham, Switzerland, 2017; pp. 373–419, ISBN 978-3-319-55621-5.
2. WHO; EML. *Model List of Essential Medicines—23rd List (2023)*; World Health Organization: Geneva, Switzerland, 2023.
3. Vardanyan, R.S.; Hruby, V.J. Antiviral Drugs. In *Synthesis of Essential Drugs*; Elsevier: Amsterdam, The Netherlands, 2006; pp. 549–557.
4. Zhai, Q.Z.; Li, X.D. Immobilization and Sustained Release of Cefalexin on MCF Nano-Mesoporous Material. *J. Dispers. Sci. Technol.* **2019**, *40*, 1675–1685. [CrossRef]
5. Ho, D.K.; Nichols, B.L.B.; Edgar, K.J.; Murgia, X.; Loretz, B.; Lehr, C.M. Challenges and Strategies in Drug Delivery Systems for Treatment of Pulmonary Infections. *Eur. J. Pharm. Biopharm.* **2019**, *144*, 110–124. [CrossRef] [PubMed]
6. Tiwari, G.; Tiwari, R.; Bannerjee, S.; Bhati, L.; Pandey, S.; Pandey, P.; Sriwastawa, B. Drug Delivery Systems: An Updated Review. *Int. J. Pharm. Investig.* **2012**, *2*, 2. [CrossRef]
7. Ghosh, S. Recent Research and Development in Synthetic Polymer-Based Drug Delivery Systems. *J. Chem. Res.* **2004**, *2004*, 241–246. [CrossRef]
8. Stebbins, N.D.; Ouimet, M.A.; Uhrich, K.E. Antibiotic-Containing Polymers for Localized, Sustained Drug Delivery. *Adv. Drug Deliv. Rev.* **2014**, *78*, 77–87. [CrossRef] [PubMed]

9. Fox, M.E.; Szoka, F.C.; Fréchet, J.M.J. Soluble Polymer Carriers for the Treatment of Cancer: The Importance of Molecular Architecture. *Acc. Chem. Res.* **2009**, *42*, 1141–1151. [CrossRef]
10. Patil, J.P.; Mahajan, H.S. A Review on Polymer Drug Conjugate—What, Why and How? *Int. J. Pharm. Sci. Res.* **2015**, *6*, 4611.
11. Yarce, C.J.; Echeverri, J.D.; Palacio, M.A.; Rivera, C.A.; Salamanca, C.H. Relationship between Surface Properties and in Vitro Drug Release from Compressed Matrix Containing Polymeric Materials with Different Hydrophobicity Degrees. *Pharmaceuticals* **2017**, *10*, 15. [CrossRef]
12. Hood, D.K.; Musa, O.M. Application of Maleic Anhydride-Based Materials. In *Handbook of Maleic Anhydride Based Materials*; Springer: Cham, Switzerland, 2016.
13. Pompe, T.; Zschoche, S.; Herold, N.; Salchert, K.; Gouzy, M.-F.; Sperling, C.; Werner, C. Maleic Anhydride Copolymers—A Versatile Platform for Molecular Biosurface Engineering. *Biomacromolecules* **2003**, *4*, 1072–1079. [CrossRef]
14. Franko, M.D.; Gates, J.E.; Ottenbrite, R.M. Synthesis and In Vitro Antimicrobial Activity of Chloramphenicol-Conjugated Copolymers. *J. Bioact. Compat. Polym.* **1990**, *5*, 283–292. [CrossRef]
15. Popescu, I.; Suflet, D.; Pelin, I.; Chiţanu, G.C. Biomedical Applications of Maleic Anhydride Copolymers. *Rev. Roum. Chim.* **2011**, *56*, 173–188.
16. Bacu, E.; Chitanu, G.C.; Couture, A.; Grandclaudon, P.; Singurel, G.; Carpov, A. Potential Drug Delivery Systems from Maleic Anhydride Copolymers and Phenothiazine Derivatives. *Eur. Polym. J.* **2002**, *38*, 1509–1513. [CrossRef]
17. McCarron, P.; Woolfson, A.; Donnelly, R.; Andrews, G.; Zawislak, A.; Price, J. Influence of Plasticiser Type and Storage Conditions on the Properties of Poly(Methyl Vinyl Ether-Co-Maleic Anhydride) Bioadhesive Films. *J. Appl. Polym. Sci.* **2004**, *91*, 1576–1589. [CrossRef]
18. Goetz, L.; Foston, M.; Mathew, A.P.; Oksman, K.; Ragauskas, A.J. Poly(Methyl Vinyl Ether-Co-Maleic Acid)–Polyethylene Glycol Nanocomposites Cross-Linked In Situ with Cellulose Nanowhiskers. *Biomacromolecules* **2010**, *11*, 2660–2666. [CrossRef] [PubMed]
19. Elizondo, E.; Córdoba, A.; Sala, S.; Ventosa, N.; Veciana, J. Preparation of Biodegradable Poly (Methyl Vinyl Ether-Co-Maleic Anhydride) Nanostructured Microparticles by Precipitation with a Compressed Antisolvent. *J. Supercrit. Fluids* **2010**, *53*, 108–114. [CrossRef]
20. Azori, M. Polymeric Prodrugs. *Crit Rev. Ther. Drug Carrier Syst.* **1987**, *4*, 39–65. [PubMed]
21. Sutekin, S.D.; Atıcı, A.B.; Guven, O.; Hoffman, A.S. Controlling of free radical copolymerization of styrene and maleic anhydride via RAFT process for the preparation of acetaminophen drug conjugates. *Radiat. Phys. Chem.* **2018**, *148*, 5–12. [CrossRef]
22. Smith, P.W.; Zuccotto, F.; Bates, R.H.; Martinez-Martinez, M.S.; Read, K.D.; Peet, C.; Epemolu, O. Pharmacokinetics of β-Lactam Antibiotics: Clues from the Past to Help Discover Long-Acting Oral Drugs in the Future. *ACS Infect. Dis.* **2018**, *4*, 1439–1447. [CrossRef] [PubMed]
23. Cakiral, K.; Sakar, D. Modification of Poly(Methyl Vinyl Ether—Alt—Maleic Anhydride) with Pregabalin Drug Active Substance via Ring Opening Polymerization of Anhydride Ring in/Noncatalyst Media. *Polym. Bull.* **2022**, *80*, 7687–7714. [CrossRef]
24. Bell, S.A. *A Beginner's Guide to Uncertainty of Measurement*; National Physical Laboratory: Teddington, UK, 2001.
25. Al-Khayri, J.M.; Asghar, W.; Akhtar, A.; Ayub, H.; Aslam, I.; Khalid, N.; Al-Mssallem, M.Q.; Alessa, F.M.; Ghazzawy, H.S.; Attimarad, M. Anthocyanin Delivery Systems: A Critical Review of Recent Research Findings. *Appl. Sci.* **2022**, *12*, 12347. [CrossRef]
26. Bisson-Boutelliez, C.; Fontanay, S.; Finance, C.; Kedzierewicz, F. Preparation and Physicochemical Characterization of Amoxicillin β-Cyclodextrin Complexes. *AAPS PharmSciTech* **2010**, *11*, 574–581. [CrossRef] [PubMed]
27. Jiang, J.; Oberdörster, G.; Biswas, P. Characterization of Size, Surface Charge, and Agglomeration State of Nanoparticle Dispersions for Toxicological Studies. *J. Nanoparticle Res.* **2009**, *11*, 77–89. [CrossRef]
28. Lockman, P.R.; Koziara, J.M.; Mumper, R.J.; Allen, D.D. Nanoparticle Surface Charges Alter Blood–Brain Barrier Integrity and Permeability. *J. Drug Target* **2004**, *12*, 635–641. [CrossRef] [PubMed]
29. Stillhart, C.; Vučićević, K.; Augustijns, P.; Basit, A.W.; Batchelor, H.; Flanagan, T.R.; Gesquiere, I.; Greupink, R.; Keszthelyi, D.; Koskinen, M.; et al. Impact of Gastrointestinal Physiology on Drug Absorption in Special Populations—An UNGAP Review. *Eur. J. Pharm. Sci.* **2020**, *147*, 105280. [CrossRef] [PubMed]
30. Koziolek, M.; Grimm, M.; Becker, D.; Iordanov, V.; Zou, H.; Shimizu, J.; Wanke, C.; Garbacz, G.; Weitschies, W. Investigation of pH and Temperature Profiles in the GI Tract of Fasted Human Subjects Using the Intellicap® System. *J. Pharm. Sci.* **2015**, *104*, 2855–2863. [CrossRef] [PubMed]
31. Danaei, M.; Dehghankhold, M.; Ataei, S.; Hasanzadeh Davarani, F.; Javanmard, R.; Dokhani, A.; Khorasani, S.; Mozafari, M. Impact of Particle Size and Polydispersity Index on the Clinical Applications of Lipidic Nanocarrier Systems. *Pharmaceutics* **2018**, *10*, 57. [CrossRef] [PubMed]
32. Zielinska, A.; Carreiró, F.; Oliveira, A.M.; Neves, A.; Pires, B.; Nagasamy Venkatesh, D.; Durazzo, A.; Lucarini, M.; Eder, P.; Silva, A.M.; et al. Polymeric Nanoparticles: Production, Characterization, Toxicology and Ecotoxicology. *Molecules* **2020**, *25*, 3731. [CrossRef] [PubMed]
33. Phan, H.; Minut, R.; McCrorie, P.; Vasey, C.; Larder, R.; Krumins, E.; Marlow, M.; Rahman, R.; Alexander, C.; Taresco, V.; et al. Role of Self-assembly Conditions and Amphiphilic Balance on Nanoparticle Formation of PEG-PDLLA Copolymers in Aqueous Environments. *J. Polym. Sci. A Polym. Chem.* **2019**, *57*, 1801–1810. [CrossRef]
34. Sandri, G.; Bonferoni, M.C.; Ferrari, F.; Rossi, S.; Caramella, C.M. The Role of Particle Size in Drug Release and Absorption. In *Particulate Products*; Springer: Cham, Switzerland, 2014; pp. 323–341.

35. Guo, M.; Wei, M.; Li, W.; Guo, M.; Guo, C.; Ma, M.; Wang, Y.; Yang, Z.; Li, M.; Fu, Q.; et al. Impacts of Particle Shapes on the Oral Delivery of Drug Nanocrystals: Mucus Permeation, Transepithelial Transport and Bioavailability. *J. Control. Release* **2019**, *307*, 64–75. [CrossRef]
36. Kamaly, N.; Yameen, B.; Wu, J.; Farokhzad, O.C. Degradable Controlled-Release Polymers and Polymeric Nanoparticles: Mechanisms of Controlling Drug Release. *Chem. Rev.* **2016**, *116*, 2602–2663. [CrossRef]
37. Zainon, S.N.M.; Azmi, W.H. Recent Progress on Stability and Thermo-Physical Properties of Mono and Hybrid towards Green Nanofluids. *Micromachines* **2021**, *2*, 176. [CrossRef] [PubMed]
38. Goscianska, J.; Ejsmont, A.; Stasiłowicz-Krzemień, A.; Sip, S.; Cielecka-Piontek, J. Enhancing Antimicrobial Activity of β-Lactam Antibiotic via Functionalized Mesoporous Carbon-Based Delivery Platforms. *Microporous Mesoporous Mater.* **2022**, *343*, 112160. [CrossRef]
39. Barba, A.A.; Bochicchio, S.; Dalmoro, A.; Caccavo, D.; Cascone, S.; Lamberti, G. Polymeric and Lipid-Based Systems for Controlled Drug Release: An Engineering Point of View. In *Nanomaterials for Drug Delivery and Therapy*; Elsevier: Amsterdam, The Netherlands, 2019; pp. 267–304, ISBN 9780128165058.
40. Joseph, E.; Singhvi, G. Multifunctional Nanocrystals for Cancer Therapy: A Potential Nanocarrier. In *Nanomaterials for Drug Delivery and Therapy*; Elsevier: Amsterdam, The Netherlands, 2019; pp. 91–116, ISBN 9780128165058.
41. Marques, M.R.C.; Loebenberg, R.; Almukainzi, M. Simulated Biological Fluids with Possible Application in Dissolution Testing. *Dissolut. Technol.* **2011**, *18*, 15–28. [CrossRef]
42. Podczeck, F.; Mitchell, C.L.; Newton, J.M.; Evans, D.; Short, M.B. The Gastric Emptying of Food as Measured by Gamma-Scintigraphy and Electrical Impedance Tomography (EIT) and Its Influence on the Gastric Emptying of Tablets of Different Dimensions. *J. Pharm. Pharmacol.* **2010**, *59*, 1527–1536. [CrossRef]
43. Balouiri, M.; Sadiki, M.; Ibnsouda, S.K. Methods for in Vitro Evaluating Antimicrobial Activity: A Review. *J. Pharm. Anal.* **2016**, *6*, 71–79. [CrossRef] [PubMed]
44. Hindler, J.A. *Analysis and Presentation of Cumulative Antimicrobial Susceptibility Test Data: Approved Guideline*; Clinical and Laboratory Standards Institute: Wayne, PA, USA, 2014; ISBN 1562388991.
45. de Souza, L.E. Poly(Vinyl Methyl Ether-Alt-Maleic Anhydride) Based Nanoparticles and Nanocapsules—Formulation and Characterization. Ph.D. Thesis, Martin-Luther-Universität Halle-Wittenberg, Halle, Germany, 2017.
46. Kaplan, E.; Ince, T.; Yorulmaz, E.; Yener, F.; Harputlu, E.; Laçin, N.T. Controlled Delivery of Ampicillin and Gentamycin from Cellulose Hydrogels and Their Antibacterial Efficiency. *J. Biomater. Tissue Eng.* **2014**, *4*, 543–549. [CrossRef]
47. Zafar, A.; Yasir, M.; Alruwaili, N.K.; Imam, S.S.; Alsaidan, O.A.; Alshehri, S.; Ghoneim, M.M.; Alquraini, A.; Rawaf, A.; Ansari, M.J.; et al. Formulation of Self-Nanoemulsifying Drug Delivery System of Cephalexin: Physiochemical Characterization and Antibacterial Evaluation. *Polymers* **2022**, *14*, 1055. [CrossRef]

Disclaimer/Publisher's Note: The statements, opinions and data contained in all publications are solely those of the individual author(s) and contributor(s) and not of MDPI and/or the editor(s). MDPI and/or the editor(s) disclaim responsibility for any injury to people or property resulting from any ideas, methods, instructions or products referred to in the content.